

Interpreting Fixed-Location Observations of Turbulence Advected by Waves: Insights from Spectral Models

JOHANNA H. ROSMAN

Institute of Marine Sciences, University of North Carolina at Chapel Hill, Morehead City, North Carolina

GREGORY P. GERBI

Physics and Geosciences Departments, Skidmore College, Saratoga Springs, New York

(Manuscript received 21 December 2015, in final form 30 January 2017)

ABSTRACT

Assigning a physical interpretation to turbulent fluctuations beneath waves is complex because eddies are advected by unsteady wave orbital motion. Here, the kinematic effects of wave orbital motion on turbulent fluctuations at a fixed location were investigated using model turbulence spatial spectra (κ spectra) together with a general form of the frozen turbulence approximation. Model autospectra and cospectra included an inertial subrange, a rolloff at energy-containing scales ($L = 2\pi/\kappa_0$), and a dissipation range. Turbulence was advected by a background flow composed of waves (rms orbital velocity σ_w , peak frequency ω_w , and spectral width $\Delta\omega_w$) propagating parallel to a current u_c . Expressions were derived for turbulence frequency spectra (ω spectra), and parameters were varied across ranges typical in the coastal ocean. Except close to the wave band, the ω -spectrum shape collapses with two dimensionless parameters, a velocity ratio σ_w/u_c , and a time-scale ratio $u_c\kappa_0/\omega_w$, which can be used to diagnose the effects of wave advection on turbulence spectra. As σ_w/u_c increases, less variance and covariance appear at low frequencies ($\omega < u_c\kappa_0$) and more appear at high frequencies ($\omega > u_c\kappa_0$). If $\sigma_w/u_c > 2$, wave advection must be taken into account when estimating turbulence length scales and integral quantities (e.g., Reynolds stress) from the low-frequency portion of spectra. The offset of the $-5/3$ region due to waves is unaffected by the rolloff or dissipation range; therefore, previously proposed methods for estimating dissipation rate from wave-affected $-5/3$ spectra are robust. Although idealized, the results inform the interpretation of turbulence ω spectra beneath waves and guide the estimation of turbulence properties from those spectra.

1. Introduction

In coastal and estuarine systems, turbulent stress gradients are leading order in momentum budgets (Geyer et al. 2000; Lentz et al. 1999). In these systems, wave orbital motion and turbulent bottom and surface boundary layers can extend over most, or all, of the water column (e.g., Feddersen et al. 2007; Jones and Monismith 2008). To quantify turbulence properties and develop and test models for mixing in these systems, it is therefore important to understand the interactions that occur between turbulence and surface waves.

Surface waves affect turbulence in a kinematical sense as well as a dynamical sense. Turbulent eddies are advected in an unsteady way by wave orbital motion;

therefore, assigning a physical interpretation to velocity and scalar fluctuation at a fixed location is complex (Lumley and Terray 1983). Additionally, a conceptual problem arises when an Eulerian framework (fixed reference frame) is used for analyzing turbulence in the presence of waves. It is therefore essential that the effects of the purely kinematic process of advection by wave orbital motion are understood and differentiated from dynamical interactions between waves and turbulence.

Advection of turbulence by wave orbital motion is particularly problematic when interpreting shallow-water turbulence measurements. In shallow water, sensors are typically mounted on moorings at fixed locations. Turbulent eddies are advected past the sensors by the background flow and turbulence properties are inferred from the resulting time series. Because time scales for advection of turbulence past a point are short

Corresponding author e-mail: Johanna Rosman, jrosman@unc.edu

compared with time scales over which turbulence evolves, the spatial structure of turbulence is inferred from time series using a frozen turbulence approximation (Taylor 1938). Thus, the spatial structure of turbulence is not observed directly but rather the distribution of energy among turbulence length scales is inferred from spectra in frequency space (ω spectra). Dissipation rates are typically estimated from $-5/3$ fits to the high-frequency (inertial subrange) portion of ω spectra. Reynolds stresses can be estimated by integrating $u'-w'$ cospectra.

Waves introduce two distinct problems when estimating turbulence statistics from this kind of data. First, when turbulent eddies are advected past sensors by wave orbital motion, the turbulence ω spectrum is difficult to interpret as it can be quite different from the corresponding spatial spectrum (κ spectrum). As a result, estimates of turbulence properties such as dissipation rate from the ω spectrum are affected dramatically by wave advection (Lumley and Terray 1983; Trowbridge and Elgar 2001; Feddersen et al. 2007). Second, the majority of the turbulence covariance is associated with energy-containing eddies and often overlaps in frequency space with the wave peak. Because wave orbital velocities can be two orders of magnitude larger than turbulent velocity fluctuations, correlations between horizontal and vertical wave orbital velocity components (wave biases) often dominate stress estimates (Shaw and Trowbridge 2001; Rosman et al. 2008). There has been considerable work on developing methods to isolate the turbulence spectrum by removing parts of the velocity signal that are correlated with surface elevation, pressure, or between velocities at different locations (Benilov and Filyushkin 1970; Shaw and Trowbridge 2001; Feddersen and Williams 2007). While these methods can remove or reduce the wave peak and often enable reasonable Reynolds stress estimates, the effects of waves can never be removed from a turbulence ω spectrum because turbulent energy is rearranged in frequency space when eddies are advected by wave orbital motion. To interpret observed ω spectra and evaluate estimates of turbulence properties, it is therefore important to understand how advection of turbulence by wave orbital motion affects turbulence ω spectra.

In this paper, we do not consider the problem of biases in estimates of integral quantities (e.g., Reynolds stress) caused by wave orbital velocities themselves. Rather, our goal is to elucidate the kinematic effects of wave advection on turbulence ω spectra. In steady currents u_c , the frequency ω of turbulent fluctuations observed at a fixed location can be converted to the effective wavenumber κ sampled using a simple form of Taylor's

frozen turbulence approximation: $\kappa = \omega/u_c$. When eddies are advected by wave orbital motion, the situation is more complex as the energy corresponding to a single-turbulence wavenumber is distributed over a range of frequencies. The effect of unsteady wave advection on the turbulence ω spectra can be investigated using a more general form of the frozen turbulence approximation. If turbulence with a known κ spectrum is advected past a fixed location by known wave and current velocities, the ω spectrum that would be observed can be calculated using a transformation between the measurement time and the effective position in the "frozen" turbulence field sampled. Using this approach, Lumley and Terray (1983) solved for the ω spectrum that would be observed if inertial subrange isotropic turbulence (Kolmogorov $-5/3$ law) was advected past a point by waves propagating parallel to a uniform current.

Lumley and Terray's (1983) results illustrate that in the presence of waves more of the turbulent energy appears at frequencies higher than the wave frequency than if the same turbulence is advected by a current alone. Therefore, dissipation rate estimates from $-5/3$ fits to the inertial subrange of ω spectra are biased (overestimated) if waves are not taken into account in the analysis. The method introduced by Lumley and Terray (1983) is commonly used to estimate dissipation rates from measured ω -spectra-containing waves and has been extended to cases in which waves propagate at an angle to the current (Trowbridge and Elgar 2001), elliptical wave orbital motion (Feddersen et al. 2007), and directionally spread waves (Gerbi et al. 2009). These methods appear to provide robust dissipation rate estimates even when wave advection is very large, as in the surfzone (Feddersen 2010, 2012).

The transformation from space (x, κ) to time (t, ω) introduced by Lumley and Terray (1983) is general and can be used to convert any spectral shape from wavenumber to frequency space using known wave and current velocities. Gerbi et al. (2008) applied this transformation to turbulence $u'-w'$ cospectra and illustrated that the distribution of turbulence covariance (Reynolds stress) in frequency space is relatively unaffected by waves if rms wave orbital velocities are less than twice the current ($\sigma_w/u_c < 2$), but the rearrangement of turbulence covariance in frequency space is significant for $\sigma_w/u_c > 2$. In that work, semitheoretical curves representing the κ -spectrum shape were fit to the low-frequency portion of turbulence cospectra, below the wave peak. These fits were extrapolated across the wave peak and higher frequencies and integrated to estimate Reynolds stresses. However, the method was limited to cases where $\sigma_w/u_c < 2$, for which the

distribution of covariance in frequency space is not significantly affected by wave orbital motion.

Here, we extend previous work that investigated the effects of wave advection on the inertial subrange part of turbulence spectra (Lumley and Terray 1983; Trowbridge and Elgar 2001; Feddersen et al. 2007) by considering a more realistic turbulence spectrum that includes a rolloff at energy-containing scales. The general frozen turbulence approach is used to transform model turbulence κ spectra to ω spectra observed at a point when the turbulence is advected by waves and current. We systematically vary the current, wave properties, and turbulence properties across a wide parameter space that spans conditions in the coastal ocean, extending the work of Gerbi et al. (2008) to cases for which wave orbital motion is large compared with the current. We then investigate how key properties of ω spectra vary across this parameter space. The results of our analyses inform the interpretation of turbulence ω spectra from a fixed location and can be used to guide the estimation of turbulence properties from those spectra.

2. Analysis framework

a. Transformation of spectra from wavenumber space to frequency space

Physically, we imagine a three-dimensional spatial field of turbulence that does not change in time. This frozen spatial field of turbulent velocity fluctuations $\mathbf{u}'(\mathbf{r})$ is advected past a sensor at position \mathbf{r}_0 by the current \mathbf{u}_c and wave orbital velocities \mathbf{u}_w . The turbulent velocity fluctuation measured by the sensor at each time t is the turbulent velocity fluctuation at position $\mathbf{r}(t) + \mathbf{r}_0$ in the spatial turbulence field, where

$$\mathbf{r}(t) = -\int_0^t \mathbf{u}_c + \mathbf{u}_w(\tau) d\tau. \quad (1)$$

Conceptually, this relationship can be used to convert the three-dimensional spatial field of turbulent velocity fluctuations to the time series of velocity fluctuations observed by a sensor at a point. Because turbulence is a stochastic process, the spatial field of turbulent velocity fluctuations is not known. However, semitheoretical models exist for turbulence spatial spectra that describe the distribution of the energy and covariance among turbulent length scales.

We begin with a turbulence spectrum in wavenumber space that is specified. The spectral tensor, denoted $\Phi_{ij}(\boldsymbol{\kappa})$, quantifies the covariance between velocity components in directions i and j per unit volume in wavenumber space $d\boldsymbol{\kappa} = (d\kappa_1, d\kappa_2, d\kappa_3)$ at a given wavenumber $\boldsymbol{\kappa} = (\kappa_1, \kappa_2, \kappa_3)$. The correlation function $R_{ij}(\mathbf{r})$, representing the correlation between

velocity components i and j at points in space separated by position vector \mathbf{r} , is by definition the inverse Fourier transform of the spectral tensor function, that is,

$$R_{ij}(\mathbf{r}) = \iiint_{\kappa_1 \kappa_2 \kappa_3} \Phi_{ij}(\boldsymbol{\kappa}) e^{i\boldsymbol{\kappa} \cdot \mathbf{r}} d\boldsymbol{\kappa}, \quad (2)$$

where the integrations are from $-\infty$ to ∞ . If turbulence with spatial representation given by Eq. (2) is advected past a sensor by a steady current \mathbf{u}_c and wave orbital velocity \mathbf{u}_w , then the effective spatial position in the turbulence field that is sampled by the sensor at time t is given by Eq. (1). Therefore, the correlation function of the measured velocity time series can be written as

$$\begin{aligned} R_{ij}(t) &= \iiint_{\kappa_1 \kappa_2 \kappa_3} \Phi_{ij}(\boldsymbol{\kappa}) e^{i\boldsymbol{\kappa} \cdot \mathbf{r}(t)} d\boldsymbol{\kappa} \\ &= \iiint_{\kappa_1 \kappa_2 \kappa_3} \Phi_{ij}(\boldsymbol{\kappa}) e^{i\kappa_1 u_c t} e^{i\boldsymbol{\kappa} \cdot \mathbf{r}_w(t)} d\boldsymbol{\kappa}, \end{aligned} \quad (3)$$

where x_1 has been defined as the direction of the current, and $\mathbf{r}_w(t)$ is the wave orbital excursion at time t . In the last step, the negative sign in the first exponent can be omitted because of symmetry.

Note that $\Phi_{ij}(\boldsymbol{\kappa})$ is a function of the turbulence only, and $\mathbf{r}_w(t)$ is a function of the waves only. If it is assumed that the waves and turbulence are independent random processes, then Eq. (3) can be written as

$$R_{ij}(t) = \iiint_{\kappa_1 \kappa_2 \kappa_3} \Phi_{ij}(\boldsymbol{\kappa}) e^{i\kappa_1 u_c t} \langle e^{i\boldsymbol{\kappa} \cdot \mathbf{r}_w(t)} \rangle d\boldsymbol{\kappa}. \quad (4)$$

The angle brackets are the expected value of the function inside the brackets at a given time t over many realizations. This term incorporates the statistical distribution of \mathbf{r}_w at a particular time t . Note that $\langle e^{i\boldsymbol{\kappa} \cdot \mathbf{r}_w(t)} \rangle$ is the characteristic function of $\mathbf{r}_w(t)$. It is therefore the inverse Fourier transform of its probability density function $p(\mathbf{r}_w)$. If it is assumed that wave orbital excursions have a Gaussian distribution, that is, $p(\mathbf{r}_w)$ is Gaussian (e.g., Wyngaard and Clifford 1977; Lumley and Terray 1983), which is true for random waves, then the characteristic function can be expressed as

$$\langle e^{i\boldsymbol{\kappa} \cdot \mathbf{r}_w(t)} \rangle = e^{-\kappa_l \kappa_m [c_{lm}(0) - c_{lm}(t)]}, \quad (5)$$

where $c_{lm}(t) = \langle r_l(t + \tau) r_m(\tau) \rangle$ is the cross-correlation function of the wave orbital excursions in directions x_l and x_m , and the angle brackets represent the expected value over all times τ . The quantity $c_{lm}(0)$ is therefore the covariance of the orbital excursion components r_l

and r_m . Although the assumption that wave orbital excursions have a Gaussian distribution breaks down in very shallow water, it is a reasonable approximation offshore of the surfzone. The assumption that fluctuations due to waves and turbulence are uncorrelated may also be poor under breaking waves. Therefore, the results should be used with caution for analysis of turbulence associated with wave breaking.

The correlation function $c_{lm}(t)$ is the inverse Fourier transform of the spectrum of wave orbital excursions $S_{r_l r_m}(\omega)$, which can be computed from the spectrum of wave orbital velocities $S_{u_i u_m}(\omega)$ as

$$c_{lm}(t) = \int_0^\infty \cos(\omega t) S_{r_l r_m}(\omega) d\omega = \int_0^\infty \cos(\omega t) \frac{S_{u_i u_m}(\omega)}{\omega^2} d\omega. \quad (6)$$

Substituting Eq. (5) into Eq. (4) yields an expression for the correlation function of the turbulent velocity fluctuations observed by the sensor as a function of the turbulence wavenumber spectrum and the wave orbital excursion statistics:

$$R_{ij}(t) = \iiint_{\kappa_1 \kappa_2 \kappa_3} \Phi_{ij}(\boldsymbol{\kappa}) e^{i\kappa_1 u_c t} e^{-\kappa_i \kappa_m [c_{lm}(0) - c_{lm}(t)]} d\boldsymbol{\kappa}. \quad (7)$$

The turbulence frequency spectrum $P_{ij}(\omega)$ can then be calculated as the Fourier transform of the turbulence correlation function $R_{ij}(t)$:

$$P_{ij}(\omega) = \frac{1}{2\pi} \int_{-\infty}^\infty e^{-i\omega t} R_{ij}(t) dt. \quad (8)$$

For any given turbulence wavenumber spectrum $\Phi_{ij}(\boldsymbol{\kappa})$ and any known current u_c and wave orbital velocity spectrum $S_{u_i u_m}(\omega)$, the spectrum of turbulent fluctuations that would be observed by a fixed sensor $P_{ij}(\omega)$ can be computed from Eqs. (6) to (8).

In this study, we consider only the simplest case of one-dimensional advection of turbulence by horizontal wave orbital velocities and a parallel current. In this case, the spatial structure of turbulence in the x_1 direction controls the temporal fluctuations observed by the sensor. Therefore, Eq. (7) can be written in terms of one-dimensional spectrum $E_{ij}(\kappa_1)$, defined as the contribution to the covariance of u_i and u_j from all wavenumbers with a κ_1 component between κ_1 and $\kappa_1 + d\kappa_1$ (see Pope 2000). The term E_{ij} is related to the spectral tensor Φ_{ij} by

$$E_{ij}(\kappa_1) = 2 \iint_{\kappa_2 \kappa_3} \Phi_{ij}(\boldsymbol{\kappa}) d\kappa_2 d\kappa_3. \quad (9)$$

For the 1D case, using Eq. (9), Eq. (7) reduces to

$$R_{ij}(t) = \frac{1}{2} \int_{-\infty}^\infty E_{ij}(\kappa_1) e^{i\kappa_1 u_c t} e^{-\kappa_1 \kappa_1 [c_{11}(0) - c_{11}(t)]} d\kappa_1 \\ = \int_0^\infty E_{ij}(\kappa_1) \cos(\kappa_1 u_c t) e^{-\kappa_1 \kappa_1 [c_{11}(0) - c_{11}(t)]} d\kappa_1. \quad (10)$$

In this study, Eqs. (6), (8), and (10) were used to transform model turbulence wavenumber spectra to frequency spectra that would be observed by a fixed sensor when the turbulence was advected by currents and wave orbital velocities with a range of peak periods and amplitudes.

b. Representation of turbulence

The transformations above were applied to semi-theoretical wavenumber spectra for both isotropic and anisotropic turbulence.

1) ISOTROPIC TURBULENCE

In isotropic turbulence, $\Phi_{ij}(\boldsymbol{\kappa})$ is completely determined by the energy spectrum because the turbulence properties are independent of direction (Pope 2000). The energy spectrum $E(\kappa)$ represents the total turbulent kinetic energy contained in wavenumbers with magnitude between κ and $\kappa + d\kappa$ and can also be thought of as $\Phi_{ij}(\boldsymbol{\kappa})$ stripped of all directional information, that is,

$$E(\kappa) = \iiint \frac{1}{2} [\Phi_{11}(\boldsymbol{\kappa}) + \Phi_{22}(\boldsymbol{\kappa}) + \Phi_{33}(\boldsymbol{\kappa})] \delta(|\boldsymbol{\kappa}| - \kappa) d\boldsymbol{\kappa}. \quad (11)$$

Note that the scalar energy spectrum $E(\kappa)$, which describes the turbulent kinetic energy as a function of wavenumber magnitude, is different from the one-dimensional spectrum tensor $E_{ij}(\kappa_1)$, which describes the covariance between two velocity components as a function of the wavenumber component in the x_1 direction. Our notation follows that of Pope (2000).

Previous work (e.g., Lumley and Terray 1983; Trowbridge and Elgar 2001) has used a Kolmogorov $-5/3$ spectrum to describe the turbulence wavenumber spectrum. Here, we use a spectrum that includes the low-wavenumber rolloff and the dissipative range (Figs. 1a,b,d,e). The spatial structure of isotropic turbulence was represented using a model spectrum with two adjustable parameters, the dissipation rate ε and the energy-containing turbulence length scale L (Pope 2000). The spectra follow the Kolmogorov $-5/3$ relationship in the inertial subrange, the low-wavenumber rolloff is controlled by L , and the high-wavenumber rolloff is controlled by the Kolmogorov length scale $\eta = (\nu^3/\varepsilon)^{1/4}$, where ν is kinematic viscosity:

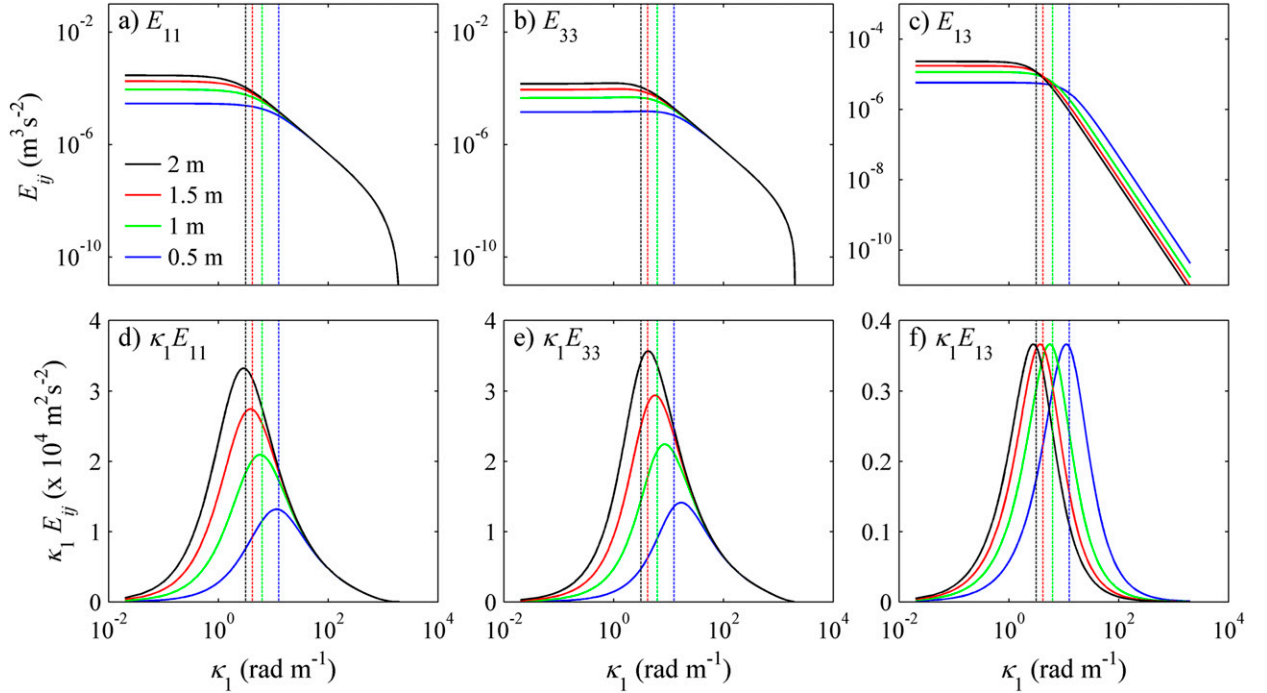


FIG. 1. Model turbulence (a),(b),(d),(e) autospectra for isotropic turbulence with $\varepsilon = 1 \times 10^{-4} \text{ m}^2 \text{ s}^{-3}$ and (c),(f) cospectra for anisotropic turbulence with Reynolds stress of $1 \times 10^{-4} \text{ m}^2 \text{ s}^{-2}$. Curves are one-dimensional spectra in the x_1 direction. Colors indicate different energy-containing length scales L and dashed lines correspond to $\kappa_0 = 2\pi/L$.

$$E(\kappa) = C\varepsilon^{2/3}\kappa^{-5/3}f_L(\kappa L)f_\eta(\kappa\eta), \quad (12)$$

$$f_L = \left\{ \frac{\kappa L}{[(\kappa L)^2 + 4\pi^2]^{1/2}} \right\}^{5/3+p_0} = \left\{ \frac{\kappa/\kappa_0}{[(\kappa/\kappa_0)^2 + 1]^{1/2}} \right\}^{5/3+p_0}$$

$$f_\eta = \exp(-c_\beta\{[(\kappa\eta)^4 + c_\eta^4]^{1/4} - c_\eta\}) \\ = \exp(-2\pi c_\beta\{[(\kappa/\kappa_\eta)^4 + (c_\eta/2\pi)^4]^{1/4} - c_\eta\}).$$

The function f_L determines the shape of the energy-containing range and tends to unity for large κ/κ_0 . Similarly, f_η describes the shape of the dissipation range and tends to unity for small κ/κ_η . We use $C = 1.5$, $p_0 = 2$, $c_\beta = 5.2$, and $c_\eta = 0.40$ (Pope 2000). We have defined $\kappa_0 = 2\pi/L$ as the wavenumber corresponding to the peak in the variance-preserving form of the energy spectrum, which differs from the definition of L used by Pope (2000).

For isotropic turbulence, the one-dimensional spectra are related to the energy spectrum by (Pope 2000)

$$E_{11}(\kappa_1) = \int_{\kappa_1}^{\infty} \frac{E(\kappa)}{\kappa} \left(1 - \frac{\kappa_1^2}{\kappa^2}\right) d\kappa \\ E_{33}(\kappa_1) = \frac{1}{2} \left[E_{11}(\kappa_1) - \kappa_1 \frac{dE_{11}}{d\kappa_1} \right]. \quad (13)$$

One-dimensional spectra were computed numerically from Eq. (13) using the form of $E(\kappa)$ in Eq. (12) (Figs. 1a,b,d,e).

2) ANISOTROPIC TURBULENCE

For the anisotropic turbulence cospectrum $E_{13}(\kappa_1)$, we used a spectrum shape proposed for the atmospheric boundary layer by Kaimal et al. (1972) and later applied to the coastal ocean bottom and surface boundary layers by Trowbridge and Elgar (2003), Feddersen and Williams (2007), and Gerbi et al. (2008):

$$E_{13}(\kappa_1) = \frac{\overline{u_1' u_3'}}{\kappa_0} \frac{7}{3\pi} \sin\left(\frac{3\pi}{7}\right) \frac{1}{1 + (\kappa_1/\kappa_0)^{7/3}}. \quad (14)$$

The shape of this spectrum is controlled by two parameters, the spatial scale of the energy-containing turbulent eddies ($2\pi/\kappa_0$), and the Reynolds stress $\overline{u_1' u_3'}$ (Figs. 1e,f). For $\kappa \gg \kappa_0$, the spectrum goes like $\kappa_1^{-7/3}$.

c. Representations of waves

The transformation of turbulence spectra from wavenumber to frequency space described in section 2a assumes that wave orbital excursions are randomly distributed. To simulate random waves, we specified the wave orbital excursion spectrum $S_{x_1 x_1}(\omega)$. It was necessary to specify the wave orbital excursion spectrum

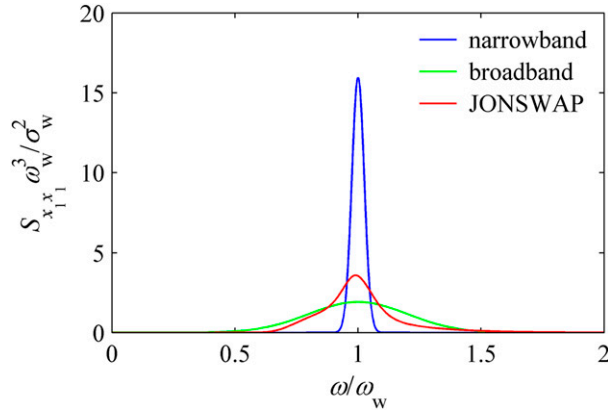


FIG. 2. Wave orbital excursion spectra used to transform turbulence spectra from wavenumber to frequency space. Spectra shown are narrowband Gaussian ($\Delta\omega_w/\omega_w = 0.025$), broadband Gaussian ($\Delta\omega_w/\omega_w = 0.2$), and a JONSWAP spectrum for fully developed waves. All spectra shown are normalized such that the integral of the corresponding orbital velocity spectrum is unity.

rather than the wave orbital velocity spectrum to avoid the wave orbital excursion spectrum blowing up at low frequencies. The wave orbital velocity spectrum is related to the wave orbital excursion spectrum by

$$S_{u_1 u_1}(\omega) = \omega^2 S_{x_1 x_1}(\omega), \quad (15)$$

and $S_{x_1 x_1}(\omega)$ was defined such that

$$\int_0^\infty S_{u_1 u_1}(\omega) d\omega = \int_0^\infty \omega^2 S_{x_1 x_1}(\omega) d\omega = \sigma_w^2. \quad (16)$$

Two different spectral shapes were used: Gaussian and JONSWAP (Fig. 2). Although real wave spectra are skewed to high frequencies, a Gaussian spectrum was used in this study so that the width of the wave peak could be controlled independently of the peak wave frequency. These spectra had the form

$$S_{x_1 x_1}(\omega) = \frac{A^2}{\sqrt{2\pi}\Delta\omega_w} \exp\left[-\frac{(\omega - \omega_w)^2}{2\Delta\omega_w^2}\right], \quad (17)$$

where $A^2 = \int_0^\infty S_{u_1 u_1}(\omega)/\omega^2 d\omega = \mu\sigma_w^2/\omega_w^2$ is the root-mean-square wave orbital excursion, $\mu = (\sigma_w/\omega_w)^{-2} \int_0^\infty S_{u_1 u_1}(\omega)/\omega^2 d\omega$ is a coefficient of order unity that depends on the shape of the wave spectrum, ω_w is the peak wave frequency, and $\Delta\omega_w$ is the width of the wave peak (one standard deviation). Two different spectral peak widths were used in the analyses: $\Delta\omega_w/\omega_w = 0.025$ (narrowband) and $\Delta\omega_w/\omega_w = 0.2$ (broadband).

To compare results for narrowband and broadband Gaussian spectra with more realistic wave distributions,

as a third case a JONSWAP spectrum was used to describe the wave heights:

$$S_{\eta\eta}(\omega) = \frac{\alpha g^2}{\omega^5} \exp\left[-\beta \frac{\omega_w^4}{\omega^4}\right] \gamma^r. \quad (18)$$

Here, α controls the spectrum amplitude, $g = 9.8 \text{ m s}^{-2}$ is acceleration due to gravity, $\beta = 1.25$ is a constant, and $\gamma = 3.3$ controls the enhancement of the wave peak relative to background. The exponent r is given by

$$r = \exp\left[-\frac{(\omega - \omega_w)^2}{2\omega_w^2 \zeta^2}\right], \quad (19)$$

where $\zeta = 0.07$ for $\omega < \omega_w$ and 0.09 for $\omega > \omega_w$.

The JONSWAP spectrum for wave heights was evaluated and converted to a spectrum for wave orbital excursions at the seafloor using the relationship from linear wave theory,

$$S_{x_1 x_1} = (\sinh\kappa h)^{-2} S_{\eta\eta}, \quad (20)$$

along with the dispersion relation $\omega^2 = g\kappa \tanh\kappa h$, where here κ is the wavenumber of the wave and h is the water depth. The coefficient α was set such that Eqs. (15) and (16) were satisfied. Although not appropriate close to the surfzone, linear wave theory has been shown to work well across the majority of the continental shelf.

The correlation function of wave orbital excursions was then computed from the wave orbital excursion spectrum using Eq. (6). The peak wave frequency ω_w as well as the magnitude of the wave spectrum σ_w was varied to investigate how wave properties affect observed turbulence frequency spectra.

d. Cases

One-dimensional spectra [$E_{11}(\kappa_1)$, $E_{33}(\kappa_1)$, $E_{13}(\kappa_1)$] for isotropic and anisotropic turbulence described in section 2b were transformed to corresponding ω spectra that would be observed at a fixed location for four different peak wave frequencies, four energy-containing turbulence length scales, and four currents (64 combinations total; Table 1). For each combination of these parameters, rms wave orbital velocities were varied from 0 up to 7 times the current ($\sigma_w/u_c = 0-7$). The parameter space included peak wave frequencies ω_w ranging from 1/8 to 8 times the frequency corresponding to advection of large turbulent eddies by the current $u_c \kappa_0$. These analyses were repeated for narrowband and broadband Gaussian wave spectra and JONSWAP wave spectra.

TABLE 1. Parameters used to generate frequency spectra observed when isotropic and anisotropic turbulence is advected past a point by parallel waves and current.

Parameters	Values
Peak wave frequency ω_w (rad s ⁻¹)	0.31, 0.63, 0.94, 1.26
Wave peak width $\Delta\omega_w/\omega_w$	0.025, 0.2
Current u_c (m s ⁻¹)	0.05, 0.1, 0.15, 0.2
Rolloff wavenumber κ_0 (rad m ⁻¹)	3.1, 4.2, 6.3, 12.6
Wave advection speed: current speed σ_w/u_c	0–7
Frequency corresponding to large eddies: wave frequency $u_c\kappa_0/\omega_w$	0.125–8
Wave orbital excursion: large eddy size $\sigma_w\kappa_0/\omega_w$	0–9

3. Results

a. Effects of wave advection on observed turbulence ω spectra

The integrals of turbulence autospectra and cospectra, which represent the total velocity component variances and covariances (Reynolds stresses), respectively, are not altered by wave orbital motion. However, as unsteady wave orbital velocities increase relative to the steady current, the shapes of observed spectra change (Figs. 3, 4). In our analyses, when rms wave orbital velocities were smaller than the current speed ($\sigma_w/u_c < 1$), ω spectra were affected little by wave orbital motion and were similar to when turbulence was advected by just a current. When rms wave orbital velocities exceeded the current speed ($\sigma_w/u_c > 1$), less variance appeared to the left of the wave frequency ($\omega < \omega_w$) and more appeared to the right of the wave frequency ($\omega > \omega_w$) than when turbulence was advected by the current alone (Figs. 3, 4). This is most easily seen in the variance-preserving spectra. When plotted on a logarithmic frequency scale, the area under these curves is proportional to each frequency band's contribution to the total variance.

The turbulence ω spectra can be divided into 1) a low-frequency part ($\omega \ll \omega_w$, $\omega < u_c\kappa_0$) in which spectral density is constant and there is an apparent rolloff that resembles the rolloff in the wavenumber spectrum at energy-containing scales, 2) an intermediate frequency part near the wave band in which spectral density oscillates with frequency, and 3) a high-frequency part ($\omega \gg \omega_w$, $\omega \gg u_c\kappa_0$) in which spectral density is increased by waves. At frequencies well above ω_w and $u_c\kappa_0$, wave advection causes a positive offset in the $-5/3$ part of the spectrum, as first described by Lumley and Terray (1983). Both the

apparent rolloff frequency and the high-frequency extent of the intermediate range vary with properties of the wave and turbulence spectra. The part of the spectrum that is altered by wave advection extends to lower frequencies for lower-frequency waves. The intermediate frequency range extends to higher frequencies as the wave frequency increases and as the wave orbital velocity increases. The same general patterns are true for both isotropic turbulence autospectra and anisotropic turbulence cospectra (Figs. 3, 4).

The shape of the wave spectrum does not significantly affect the low- or high-frequency behavior of the observed turbulence spectrum; however, it strongly affects the spectrum shape close to the wave peak, in the intermediate frequency range (Fig. 5). The narrower the wave peak, the larger the magnitude of oscillations in the turbulence ω spectrum near the wave peak. Although these oscillations have a large effect on the value of the spectrum at a given frequency near the wave band, their effect on the integral of the spectrum is minimal; therefore, the shape of integrated turbulence spectrum is almost independent of the shape of the wave spectrum.

b. Dimensionless parameters controlling the shapes of observed spectra

Expressions for the shapes of observed ω spectra can be derived by substituting the expressions for model κ spectra [Eqs. (12)–(14)] into the equations used to transform spectra from wavenumber to frequency space [Eqs. (6), (8), (10)]. Variables in the equations (κ_1 , t , ω) are then arranged into dimensionless variables [$\omega/(u_c\kappa_0)$, $s = \kappa_1/\kappa_0$, and $y = u_c\kappa_0 t$], where $\omega/(u_c\kappa_0)$ is dimensionless frequency, and s and y are integration variables, resulting in expressions for ω spectra in terms of dimensionless parameter groups. The shape of the dissipation range has negligible effect on the ω spectrum, except for very large values of $\omega/(u_c\kappa_0)$, corresponding to very small, high-frequency fluctuations that are typically not resolved in field measurements. Over the frequency range relevant to field measurements, $f_\eta = 1$, and the shape of the ω spectrum is independent of $\kappa_0\eta$. We therefore take $f_\eta = 1$ in our theoretical analyses. Derivations are provided in the appendix.

The resulting expression for the two-sided u_1 auto-spectrum for isotropic turbulence is

$$P_{11}(\omega) = \left(\frac{\varepsilon}{\kappa_0}\right)^{2/3} \frac{1}{u_c\kappa_0} F_3\left(\frac{\omega}{u_c\kappa_0}, \frac{u_c\kappa_0}{\omega_w}, \frac{\sigma_w}{u_c}, \mu\right), \quad (21)$$

where

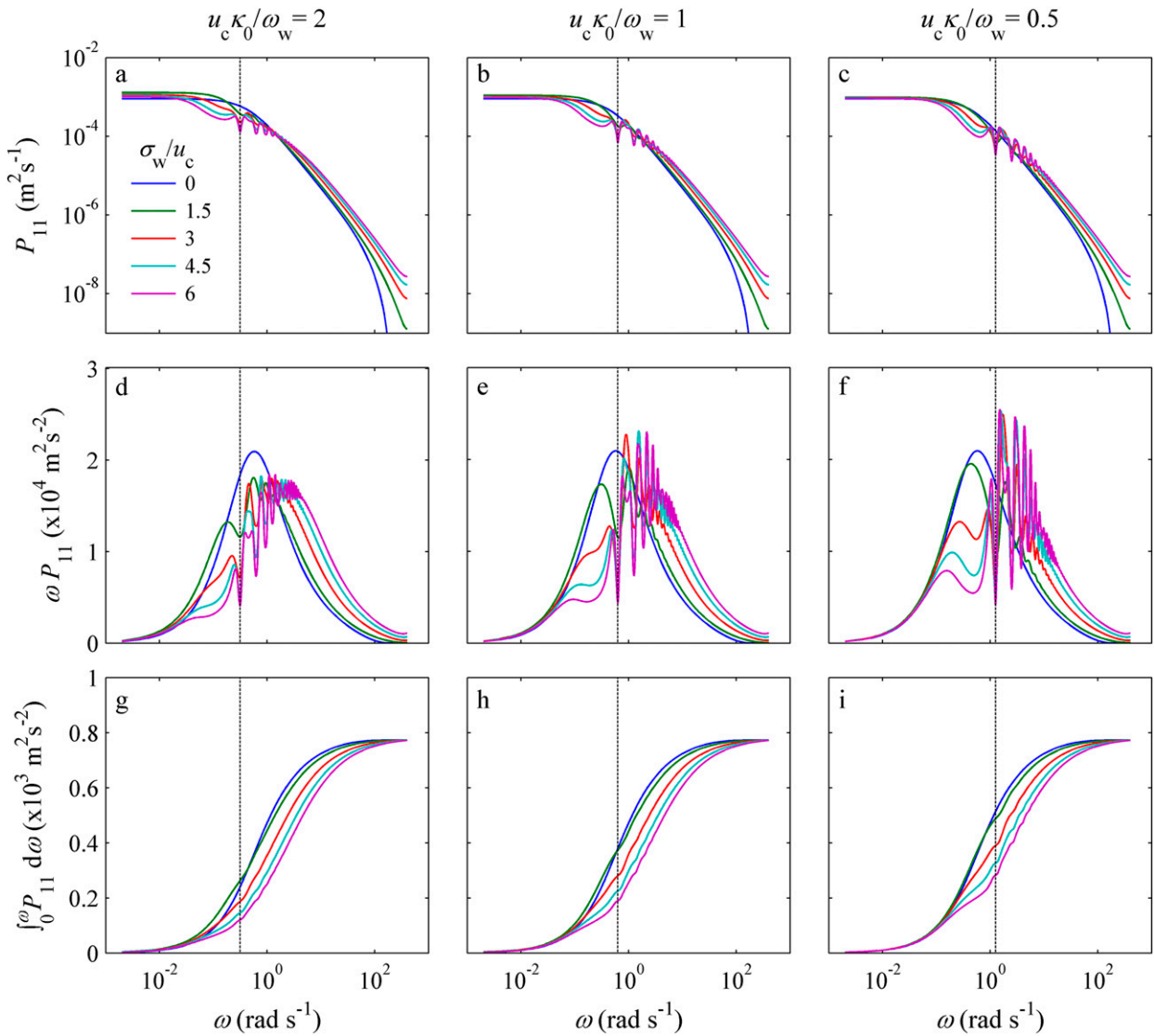


FIG. 3. Example isotropic turbulence autospectra in frequency space, showing the effect of increasing wave orbital velocities. Colors indicate different ratios of rms wave orbital velocity to current (σ_w/u_c). Rows are (top) spectra, (middle) variance-preserving spectra, and (bottom) integrated spectra. Columns are (left) low, (center) medium, and (right) high-frequency waves. Dashed vertical lines indicate the wave frequency. All cases shown correspond to the narrowband wave spectrum.

$$F_3\left(\frac{\omega}{u_c \kappa_0}, \frac{u_c \kappa_0}{\omega_w}, \frac{\sigma_w}{u_c}, \mu\right) = \frac{C}{4\pi} \int_{-\infty}^{\infty} \int_{-\infty}^{\infty} F_1(s) e^{-i[\omega/(u_c \kappa_0) - s]y} e^{-[(u_c \kappa_0)/\omega_w]^2 (\sigma_w/u_c)^2 [\mu - F_2(y)]s^2} ds dy,$$

$$F_2(y) = \frac{c_{11}(t)}{(\sigma_w/\omega_w)^2} = \left(\frac{\omega_w}{u_c \kappa_0}\right)^2 \int_0^{\infty} e^{i[\omega/(u_c \kappa_0)]y} \frac{S_{u_1 u_1}^*[\omega/(u_c \kappa_0)]}{[\omega/(u_c \kappa_0)]^2} d[\omega/(u_c \kappa_0)],$$

$$\mu = \left(\frac{\sigma_w}{\omega_w}\right)^{-2} \int_0^{\infty} \frac{S_{u_1 u_1}(\omega)}{\omega^2} d\omega, \quad \text{and}$$

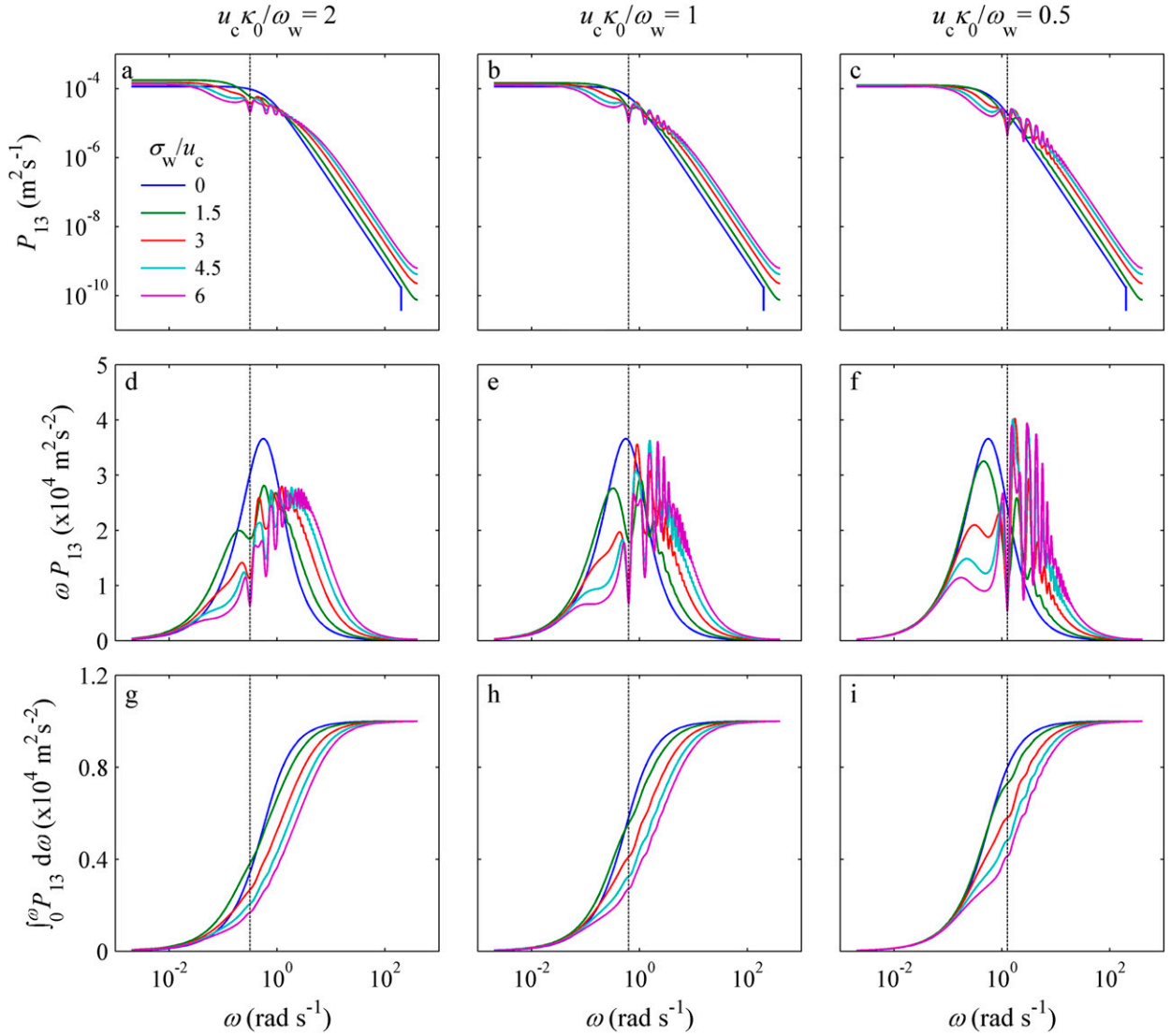


FIG. 4. As in Fig. 3, but for anisotropic turbulence cospectra in frequency space, showing the effect of increasing wave orbital velocities on observed spectra.

$$F_1(s) = \int_s^\infty \frac{s'}{(s'^2 + 1)^{11/6}} \left(1 - \frac{s^2}{s'^2}\right) ds'.$$

For the u_3 autospectrum P_{33} , the same equations apply except that F_1 is replaced by G_1 :

$$G_1(s) = \frac{1}{2} \int_s^\infty \frac{s'}{(s'^2 + 1)^{11/6}} \left(1 + \frac{s^2}{s'^2}\right) ds'. \quad (22)$$

The magnitude of the spectrum is proportional to $(\varepsilon/\kappa_0)^{2/3}/(u_c \kappa_0)$, while the spectrum shape is described by the function F_3 . The ω -spectrum shape therefore depends primarily on the two parameters $u_c \kappa_0/\omega_w$ and

σ_w/u_c . Near the peak wave frequency, the ω spectrum is also affected by $S_{u_1 u_1}^*$, the wave orbital velocity spectrum defined as a function of $\omega/(u_c \kappa_0)$ and normalized such that $\int_0^\infty S_{u_1 u_1}^*[\omega/(u_c \kappa_0)] d[\omega/(u_c \kappa_0)] = 1$ (see the appendix).

The corresponding expressions for the cospectrum for anisotropic turbulence are

$$P_{13}(\omega) = \frac{\overline{u'_1 u'_3}}{u_c \kappa_0} H_3 \left(\frac{\omega}{u_c \kappa_0}, \frac{u_c \kappa_0}{\omega_w}, \frac{\sigma_w}{u_c}, \mu \right), \quad (23)$$

where

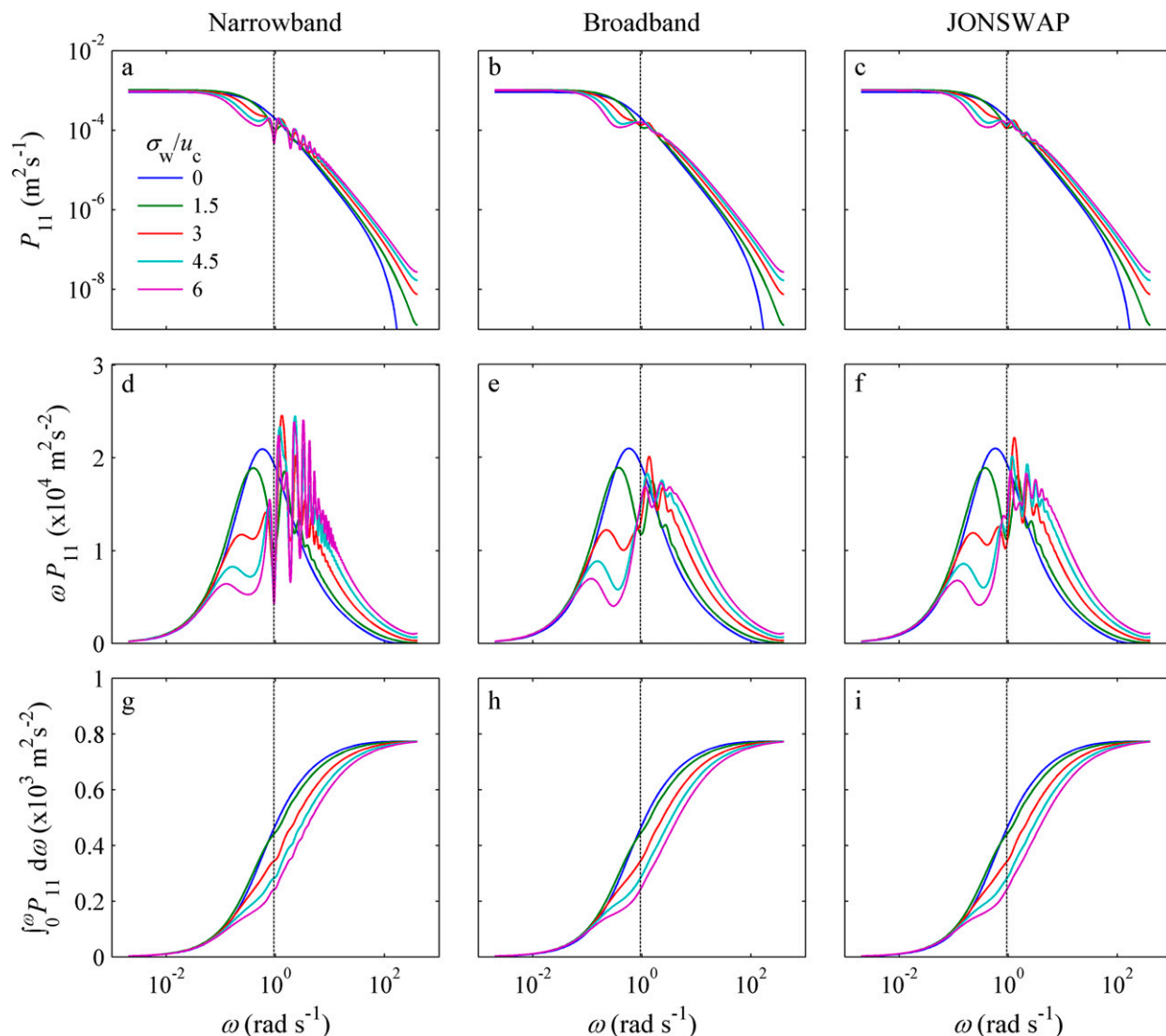


FIG. 5. Example isotropic turbulence autospectra in frequency space, showing the effect of wave spectrum shape on observed turbulence spectra. For these examples, $u_c \kappa_0 / \omega_w = 0.67$. Colors indicate different ratios of rms wave orbital velocity to current (σ_w / u_c). (left) Narrowband, (center) broadband, and (right) JONSWAP wave spectra. Dashed vertical lines indicate the peak wave frequency.

$$H_3 \left(\frac{\omega}{u_c \kappa_0}, \frac{u_c \kappa_0}{\omega_w}, \frac{\sigma_w}{u_c}, \mu \right) = \frac{7}{12\pi^2} \sin \left(\frac{3\pi}{7} \right) \int_{-\infty}^{\infty} \int_{-\infty}^{\infty} \frac{1}{1 + |s|^{7/3}} e^{-i[\omega/(u_c \kappa_0) - s]y} e^{-[(u_c \kappa_0 / \omega_w)^2 (\sigma_w / u_c)^2 [\mu - F_2(y)]s]^2} ds dy,$$

and F_2 and μ are defined in Eq. (21).

The shapes of both turbulence autospectra and cospectra in frequency space are controlled primarily by the same two parameters: $u_c \kappa_0 / \omega_w$ and σ_w / u_c . The first parameter $u_c \kappa_0 / \omega_w$ represents the ratio of the frequency corresponding to the low-wavenumber rolloff in the turbulence spectrum in the absence of waves $u_c \kappa_0$ to the peak wave frequency ω_w . The second

parameter σ_w / u_c is the ratio of the rms advection speed by waves to the advection speed by current. A third parameter $\sigma_w \kappa_0 / \omega_w$, representing the ratio of the rms wave orbital excursion to the spatial scale of energy-containing eddies, can be formed from the product of $u_c \kappa_0 / \omega_w$ and σ_w / u_c . Equations (21)–(23) can be rewritten in terms of any two of these three dimensionless parameters.

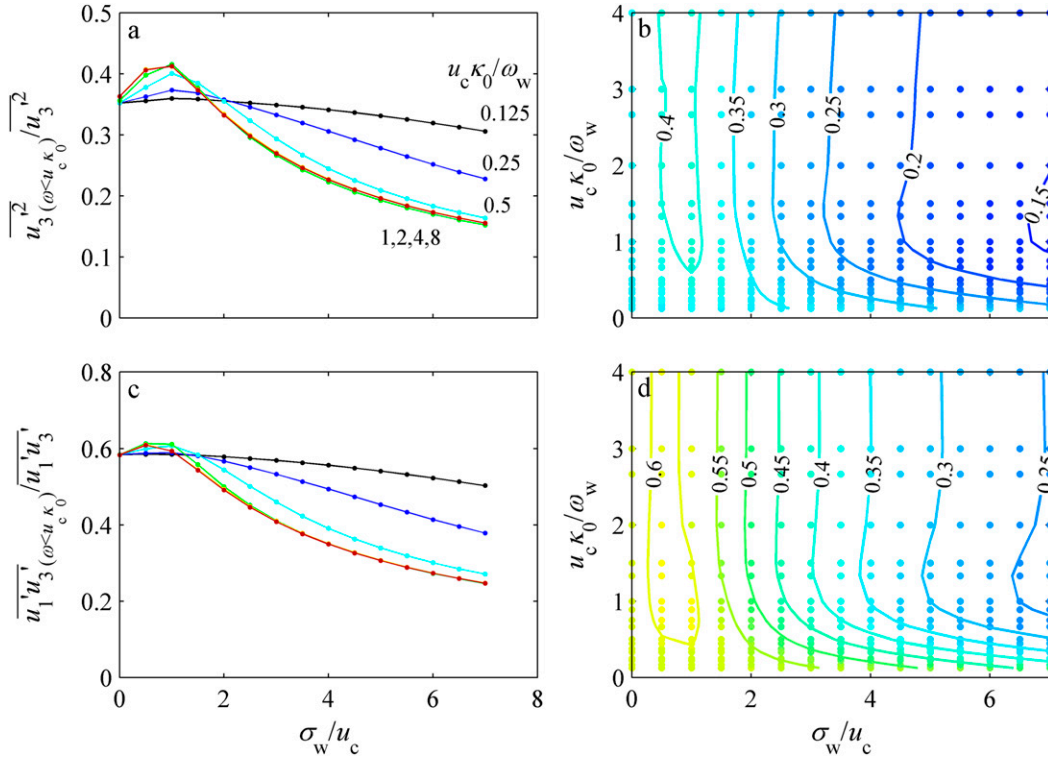


FIG. 6. Fraction of total (top) u_3^2 variance and (bottom) u_1-u_3 covariance that appears in the spectrum at frequencies less than the frequency corresponding to energy-containing turbulence advected by the current $u_c \kappa_0$ for a range of wave conditions and turbulence properties. Results shown correspond to a broadband Gaussian wave spectrum. (left) Plots of variance or covariance fraction vs velocity ratio σ_w/u_c . Colors indicate different values of the time-scale ratio $u_c \kappa_0/\omega_w$. (right) Contours of variance and covariance fraction vs the velocity and time-scale ratios.

When the fraction of the variance and covariance appearing in the spectrum at frequencies less than the frequency corresponding to advection of energy-containing turbulence by the current $u_c \kappa_0$ is plotted against σ_w/u_c , the results collapse according to $u_c \kappa_0/\omega_w$ (Figs. 6a,c). However, the results become independent of $u_c \kappa_0/\omega_w$ for $u_c \kappa_0/\omega_w > 1$, which corresponds to wave frequencies in the flat part of the turbulence spectrum, below the turbulence rolloff frequency. That is, for $u_c \kappa_0/\omega_w > 1$, the fraction of the turbulent energy below $\omega = u_c \kappa_0$ is independent of the wave frequency and is a function only of σ_w/u_c .

When instead the fraction of the total variance and covariance appearing in the spectrum at frequencies less than the peak wave frequency is plotted against σ_w/u_c , the results collapse again according to the value of $u_c \kappa_0/\omega_w$ (Figs. 7a,c). When the variance and covariance fraction below the wave frequency are plotted against $\sigma_w \kappa_0/\omega_w$, results for all 64 parameter combinations collapse onto a single curve for high values of $\sigma_w \kappa_0/\omega_w$ (Figs. 7b,d). Curves for different $u_c \kappa_0/\omega_w$ values collapse onto this curve when $\sigma_w \kappa_0/\omega_w > 2u_c \kappa_0/\omega_w$,

corresponding to $\sigma_w/u_c > 2$, that is, when the average speed at which turbulence is advected past a point is dominated by wave orbital motion rather than current. This means that the fraction of the variance or covariance below the peak wave frequency depends only on wave properties and is independent of the current if $\sigma_w/u_c > 2$.

c. Properties of ω spectra and dependence on dimensionless parameters

We now consider how turbulence ω -spectrum shapes vary with the above dimensionless parameters, focusing on properties that are relevant to interpreting observations and estimating turbulence parameters. The dependences of spectrum properties on dimensionless parameters are summarized in Table 2.

1) INERTIAL SUBRANGE ($\omega > 10u_c \kappa_0$, $\omega > 10\omega_w$)

For frequencies much higher than both the wave frequency and the frequency corresponding to advection of energy contain eddies by the current, the spectral energy is increased by wave advection, and there is a positive

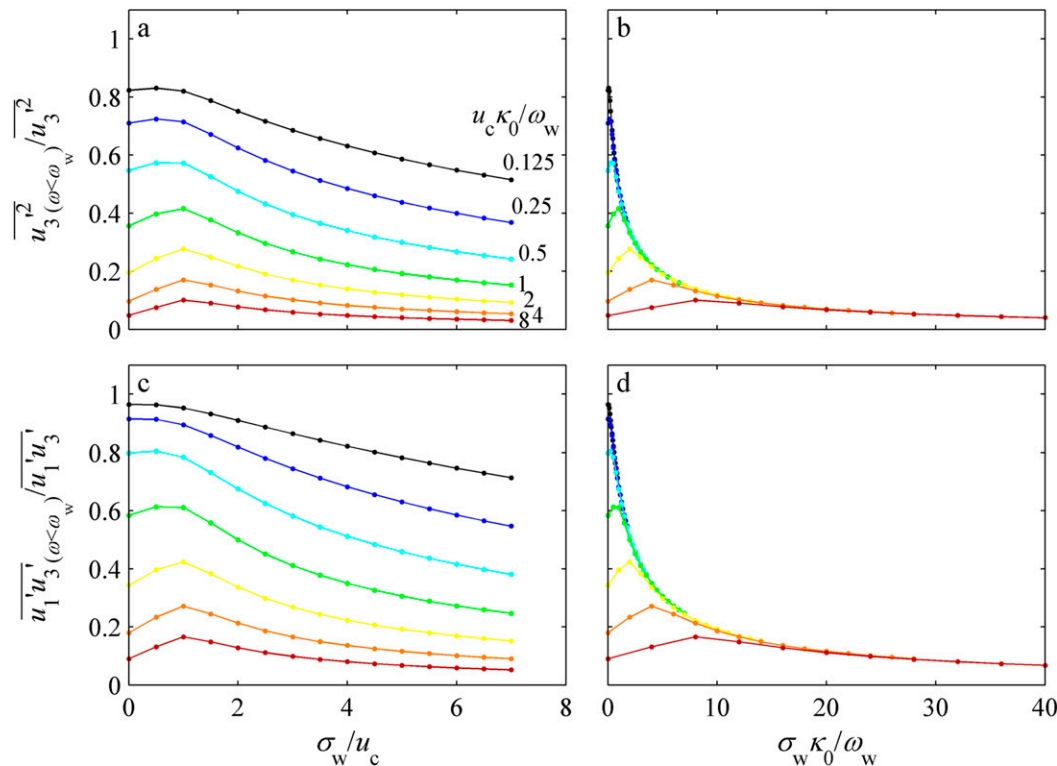


FIG. 7. Fraction of (top) total u_3^2 variance and (bottom) $u_1^2-u_3^2$ covariance that appears in the spectrum at frequencies less than the wave frequency for a range of wave conditions and turbulence properties. Results shown correspond to a broadband Gaussian wave spectrum. Panels are plots of variance or covariance fraction vs (left) wave to current velocity ratio and (right) ratio of rms wave orbital excursion to energy-containing turbulence length scale. Colors indicate different values of the time-scale ratio $u_c \kappa_0 / \omega_w$.

offset in the spectrum (e.g., Fig. 4), as first described by Lumley and Terray (1983). Eddies that appear in the spectrum at these frequencies have length scales much smaller than the wave orbital excursion ($\kappa \gg \omega_w / \sigma_w$). Wave orbital motion together with the current determines the speed at which they are advected past a sensor. The advection speed varies over a wave cycle; therefore, energy corresponding to a single-turbulence wavenumber κ is spread across a range of frequencies. For $\kappa > \kappa_0$, there is a rapid decrease in the turbulent energy with increasing κ . Additionally, for $\sigma_w / u_c > 1$, waves increase the time-averaged advection speed. The net result is that turbulent energy is observed at higher frequencies in the presence of waves than when the turbulence is advected by just a current. For this reason, there is a positive offset in the inertial subrange part of the spectrum relative to when there are no waves.

The offset in the high-frequency range of autospectra has previously been described using a factor I that multiplies the expression for the $-5/3$ region in the absence of waves (Trowbridge and Elgar 2001):

$$\begin{aligned} P_{11,\text{inertial}}(\omega) &= (18/55) C \varepsilon^{2/3} u_c^{2/3} \omega^{-5/3} I \\ P_{33,\text{inertial}}(\omega) &= (24/55) C \varepsilon^{2/3} u_c^{2/3} \omega^{-5/3} I. \end{aligned} \quad (24)$$

If a $\kappa^{-5/3}$ spectral shape is assumed for all wavenumbers, then an expression for I can be derived by taking the high-frequency limit of Eq. (21) (see the appendix). For parallel waves and current, the expression is (see also Trowbridge and Elgar 2001)

$$I = \frac{1}{\sqrt{2\pi}} \int_{-\infty}^{\infty} \left(1 - \frac{\sigma_w}{u_c} \chi\right)^{2/3} e^{-(1/2)\chi^2} d\chi. \quad (25)$$

The offset in the $-5/3$ part of the spectrum affects the estimation of dissipation rates from fits to the high-frequency portion of autospectra; correction of dissipation estimates is relatively straightforward.

Similar expressions can be derived for the high-frequency limit of anisotropic turbulence cospectra, although the dissipation rate cannot be calculated from the anisotropic cospectrum. At high wavenumbers, the cospectrum has a $\kappa^{-7/3}$ shape; therefore, cospectra,

TABLE 2. Summary of dependence of spectrum properties on dimensionless parameters.

	High-frequency waves	Low-frequency waves
	$u_c \kappa_0 / \omega_w < 1$ $\sigma_w / u_c < 1$	$u_c \kappa_0 / \omega_w > 1$ $\sigma_w / u_c < 1$
Fraction of variance in $\omega < u_c \kappa_0$ (Fig. 6)	$u_c \kappa_0 / \omega_w$	σ_w / u_c
Fraction of variance in $\omega < \omega_w$ (Fig. 7)	$u_c \kappa_0 / \omega_w$ and σ_w / u_c	$u_c \kappa_0 / \omega_w$ and σ_w / u_c
Offset of $-5/3$ and $-7/3$ regions (Fig. 8)	σ_w / u_c	σ_w / u_c
VP spectrum high-frequency peak (ω_{peak} ; Fig. 9)	$u_c \kappa_0$, if $\sigma_w \kappa_0 / \omega_w > 2$	$u_c \kappa_0$, if $\sigma_w \kappa_0 / \omega_w > 2$
Very low-frequency offset (Fig. 10)	N/A (no offset)	N/A (no offset)
Apparent rolloff frequency (ω_{90} ; Fig. 11)	$u_c \kappa_0$ $(\sigma_w / u_c)^{-1} \omega_w$, if $\sigma_w \kappa_0 / \omega_w > 1$	$u_c \kappa_0$ $(\sigma_w / u_c)^{-1} \omega_w$, if $\sigma_w \kappa_0 / \omega_w > 1$

when plotted on log scales, have $-7/3$ slopes for high frequencies. Wave advection causes an offset in the $-7/3$ part of the ω spectrum that is analogous to the offset in the $-5/3$ region in autospectra. The offset is also a function of one parameter σ_w / u_c . It can be shown (see the appendix) that, for $\omega \gg \omega_w$ and $\omega \gg u_c \kappa_0$, Eq. (23) reduces to

$$P_{13,\text{inertial}}(\omega) = \overline{u_1' u_3'} (u_c \kappa_0)^{4/3} \frac{7}{6\pi} \sin\left(\frac{3\pi}{7}\right) \omega^{-7/3} J, \quad (26)$$

where

$$J = \frac{1}{\sqrt{2\pi}} \int_{-\infty}^{\infty} \left(1 - \frac{\sigma_w}{u_c} \chi\right)^{4/3} e^{-(1/2)\chi^2} d\chi. \quad (27)$$

The functional forms of I and J differ due to the different exponent of κ in the κ spectrum.

We evaluated the accuracy of these relationships for spectra that include a low-frequency rolloff (Fig. 1) by fitting lines with $-5/3$ and $-7/3$ slopes to the inertial subranges of computed autospectra and cospectra on logarithmic axes. For the autospectra, we present results only for vertical velocities. Similar results were obtained in our analyses of horizontal velocities. In each case, the start and end points for the fit were determined from the start and end points of the inertial subrange of the corresponding κ spectrum. The low-frequency end point was chosen to be the larger of $\kappa_{\text{lf}}(u_c + \sigma_w)$, where κ_{lf} was the start of the $-5/3$ (or $-7/3$) region in the κ spectrum and $10\omega_w$. The term $\kappa_{\text{lf}}(u_c + \sigma_w)$ corresponds to advection of the largest eddies in the inertial subrange at the speed $u_c + \sigma_w$, which is only exceeded 15% of the time for random waves. The high-frequency end point was chosen to be $\omega_{\text{hf}} = \kappa_{\text{hf}}(u_c + \sigma_w)$, where κ_{hf} was the start of the dissipation range for autospectra and the Nyquist wavenumber for cospectra. End points $\omega_{\text{lf}} < 10\omega_w$ and $\omega_{\text{hf}} > \omega_N/8$, where ω_N is the Nyquist frequency, were not allowed.

The factors I and J were computed from spectral fits for different current speeds, wave amplitudes, wave frequencies, and turbulence length scales (Fig. 8). Both I and J were a function of one variable σ_w / u_c and were independent of wave frequency and turbulence length scale (Fig. 8), confirming that the low-wavenumber rolloff in the turbulence κ spectrum has negligible effect on the $-5/3$ (or $-7/3$) part of the ω spectrum for the range of conditions considered in this study. Results from the fits to autospectra agreed well with the analytical solution of Trowbridge and Elgar (2001), which was derived for a Kolmogorov $-5/3$ κ spectrum with no rolloff or

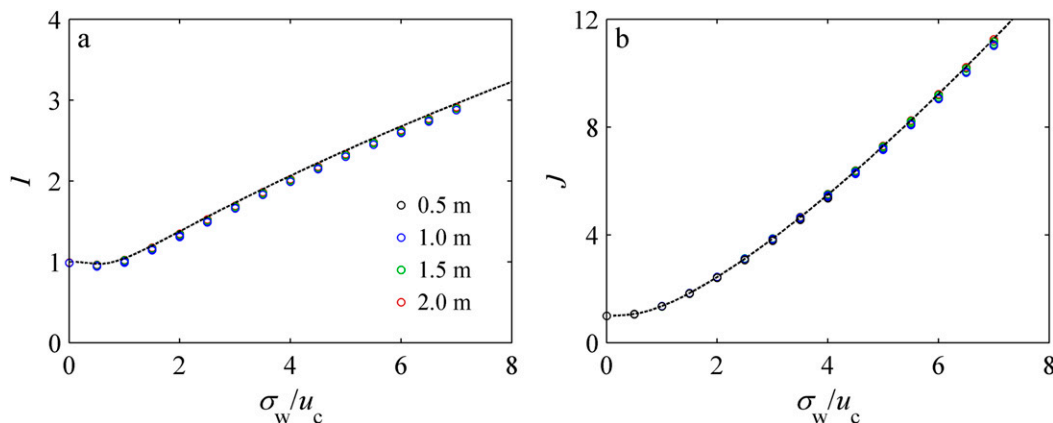


FIG. 8. Offset of (a) the $-5/3$ region of autospectra and (b) the $-7/3$ region of cospectra due to advection of turbulence by waves. Results shown correspond to a broadband Gaussian wave spectrum. Circles are plots of the parameters I [Eq. (24)] and J [Eq. (26)] determined from fits to frequency spectra. Colors indicate turbulence length scale, which determines the length of the inertial subrange. Results for different turbulence length scales are almost indistinguishable, indicating that I and J depend only on σ_w/u_c . The dashed lines are the analytical forms for the functions I [Eq. (25)] and J [Eq. (27)].

dissipation range. Therefore, dissipation estimates from Eqs. (24) and (25) are expected to be robust and independent of details of the turbulence spectrum and wave spectrum as long as the inertial subrange spans a sufficient wavenumber range. Results from fits to cospectra also agreed well with the theoretical solution [Eq. (27)].

2) INTERMEDIATE FREQUENCY RANGE ($0.5\omega_w < \omega < 10\omega_w$)

In the intermediate-frequency range close to the wave peak, the shape of the turbulence ω spectrum is complex and depends on the shape of the wave spectrum. For narrowband waves, there are large distinct fluctuations in spectral density from $0.5\omega_w$ to $10\omega_w$, with dips in spectral density at harmonics of the peak wave frequency (Figs. 3, 4). The amplitude of these fluctuations increases with increasing σ_w/u_c . The fluctuations are smaller and less well-defined for broadband waves (Fig. 5).

As shown by Lumley and Terray (1983), the frequency spectrum resulting from advection of turbulence by monochromatic waves with no current is a line spectrum that can be represented as the sum of delta functions at harmonics of the wave frequency. For waves with finite spectral width, the turbulence frequency spectrum is a sequence of finite-width peaks, centered at harmonics of the peak wave frequency. The broader the wave spectrum, the broader are the peaks in the turbulence spectrum and the more overlap occurs between consecutive harmonics. When a current occurs with monochromatic waves,

the line peaks at harmonics of the wave frequency are broadened, and there is a singularity at harmonics of the wave frequency (Lumley and Terray 1983). For waves with finite spectral width, these singularities become “dips” in the turbulence frequency spectrum. Therefore, the oscillations in the turbulence spectrum are larger for larger σ_w/u_c and also larger and more well-defined for narrower wave spectra (smaller $\Delta\omega_w/\omega_w$; Fig. 5).

3) HIGH-FREQUENCY PEAK IN VARIANCE-PRESERVING SPECTRUM ($2u_c\kappa_0 < \omega < 10u_c\kappa_0$, $\omega > 2\omega_w$)

Although there are large fluctuations in the turbulence ω spectrum at frequencies close to the wave peak ($0.5\omega_w < \omega < 10\omega_w$; see previous section), there are some general trends in the underlying spectrum shape within this frequency range. For all cases where the wave orbital excursion is larger than the energy-containing turbulent eddies ($\sigma_w\kappa_0/\omega_w > 2$), wave advection results in a shift of the turbulence rolloff (or peak in variance-preserving spectrum) to higher frequencies (e.g., Figs. 3, 4, left column). This is because energy-containing length scales are smaller than the wave orbital excursion; therefore, wave orbital motion increases the speed at which eddies, from energy-containing scales through the inertial subrange, are advected past the sensor. The bulk of the turbulence spectrum, from the rolloff through the inertial subrange, is therefore shifted to higher frequencies. If $\sigma_w\kappa_0/\omega_w < 2$, there is not a well-defined, high-frequency peak in the variance-preserving spectrum.

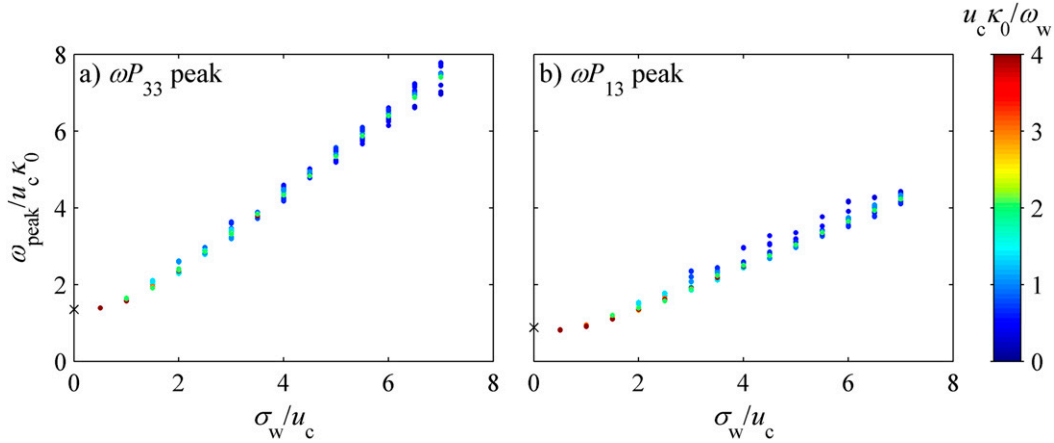


FIG. 9. Frequency of high-frequency peak in variance-preserving turbulence ω spectra vs wave to current velocity ratio. Results shown correspond to a broadband Gaussian wave spectrum. Peaks in (a) u_3^2 autospectra and (b) $u_1 u_3^2$ cospectra. Colors indicate values of the parameter $u_c \kappa_0 / \omega_w$. Only spectra with a well-defined peak in the range $\omega > \omega_w$ are shown, which correspond to cases where the wave orbital excursion is large compared with energy-containing turbulence ($\sigma_w \kappa_0 / \omega_w > 2$).

For each spectrum that satisfied the condition $\sigma_w \kappa_0 / \omega_w > 2$, the frequency of the peak in the variance-preserving spectrum ω_{peak} was estimated by smoothing the variance-preserving spectrum to remove oscillations and selecting the frequency that corresponded to the maximum in the smoothed spectrum. For $\sigma_w / u_c < 1$, the frequency of the peak is unaffected by wave advection and $\omega_{\text{peak}} \sim 2 u_c \kappa_0$. For $\sigma_w / u_c > 1$, $\omega_{\text{peak}} / u_c \kappa_0$ increases linearly with σ_w / u_c (Fig. 9). This translates to an ω_{peak} proportional to $\sigma_w \kappa_0$, corresponding to advection of energy-containing eddies at the rms wave orbital velocity. The dimensionless peak frequency $\omega_{\text{peak}} / u_c \kappa_0$ increases more slowly with σ_w / u_c for cospectra than for autospectra due to the more rapid decline in

spectral energy with increasing wavenumber in cospectra. These results suggest that if the wave orbital excursion is long compared with energy-containing length scales ($\sigma_w \kappa_0 / \omega_w > 2$), energy-containing turbulence length scales ($L = 2\pi / \kappa_0$) can be estimated from the peak frequency in the variance-preserving turbulence ω spectrum ω_{peak} together with the ratio of the wave orbital velocity to current σ_w / u_c .

4) LOW-FREQUENCY RANGE ($\omega < 0.5\omega_w, \omega < u_c \kappa_0$)

The shapes of the low-frequency parts of both autospectra and cospectra resemble those in the absence of waves (Figs. 3, 4, 5). At very low frequencies, the spectrum is flat and spectral density does not vary with

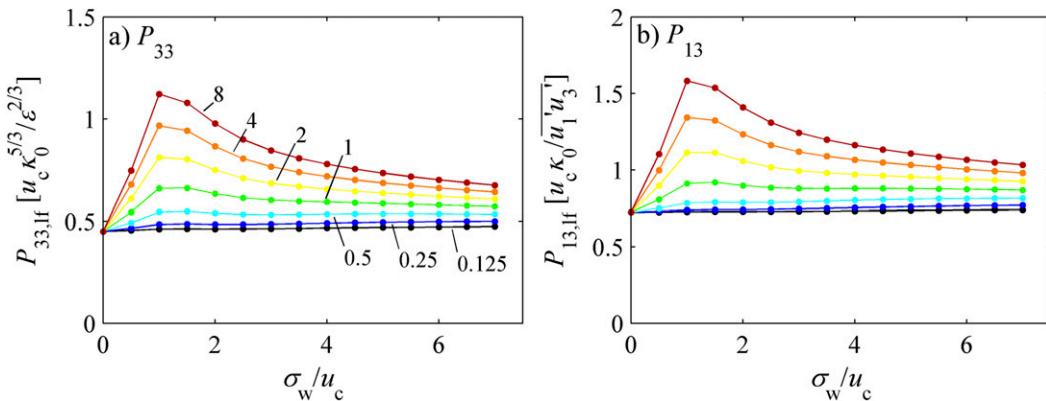


FIG. 10. Value of spectral density function in the very low-frequency part of the spectrum, below the apparent rolloff frequency, vs wave to current velocity ratio. Results shown correspond to a broadband Gaussian wave spectrum. Panels correspond to (a) the autospectrum and (b) the cospectrum. Colors indicate different values of $u_c \kappa_0 / \omega_w$.

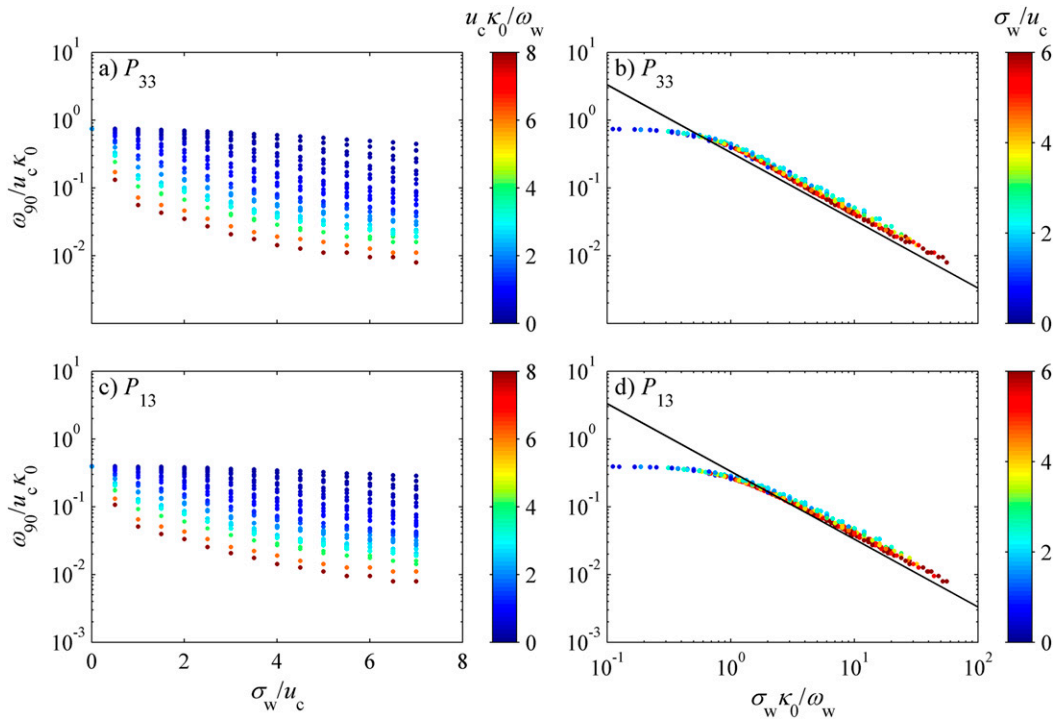


FIG. 11. Frequency of apparent low-frequency rolloff. Panels are frequency (ω_{90}) below which (top) the u_3^2 autospectrum and (bottom) the u_1^2 – u_3^2 cospectrum differs from the value in the low-frequency flat part of the spectrum by less than 10%. Results are plotted vs (left) ratio of wave orbital velocity to current and (right) ratio of wave orbital excursion to energy-containing eddy size. The black lines in (b) and (d) are the relationship in Eq. (29).

frequency (Figs. 3, 4, 5). We denote the spectral density in this frequency range as $P_{33,\text{lf}}$. The value of $P_{33,\text{lf}}$ increases as σ_w/u_c increases from 0 to 1 and then decays as σ_w/u_c increases further (Fig. 10a). The offset in $P_{33,\text{lf}}$ associated with waves is greatest for large $u_c\kappa_0/\omega_w$ and reduces to zero for $u_c\kappa_0/\omega_w < 1$. The same pattern occurs for $P_{13,\text{lf}}$.

The rolloff in the spectrum appears to be shifted to lower frequencies as wave orbital velocities increase (Figs. 3, 4, 5). The frequency of this apparent rolloff was estimated as ω_{90} , the frequency above which the spectral density is less than 90% of its value in the very low frequency, flat part of the spectrum. The apparent rolloff frequency was determined empirically from computed spectra and is plotted versus parameters that control the spectral shape in Fig. 11. The apparent rolloff frequency decreases as σ_w/u_c increases (Figs. 11a,c). This effect is more extreme when $u_c\kappa_0/\omega_w$ is larger, that is, when the wave frequency is lower relative to the frequency corresponding to advection of energy-containing eddies by the current. When ω_{90} is plotted against $\sigma_w\kappa_0/\omega_w$ the results collapse onto a single curve (Figs. 11b,d), illustrating that the low-frequency spectral shape, in

dimensionless form, is determined primarily by the ratio of wave orbital excursion to energy-containing turbulence length scale. There are small deviations from this curve according to the value of σ_w/u_c . The apparent rolloff frequency is constant and independent of $\sigma_w\kappa_0/\omega_w$ when $\sigma_w\kappa_0/\omega_w < 1$ (Figs. 11b,d), corresponding to cases where the wave orbital excursion is smaller than the size of energy-containing eddies, and therefore the frequency at which energy-containing eddies appear in the spectrum is not altered by wave advection.

It can be shown that in the limit of frequencies much lower than the wave frequency ($\omega \ll \omega_w$), if $\sigma_w\kappa_0/\omega_w > 1$, Eqs. (21) and (23) reduce to (see the appendix)

$$P_{33}(\omega) = e^{-\mu[(\sigma_w\kappa_0)/\omega_w]^2[\omega/(u_c\kappa_0)]^2} P_{33,\text{lf}} = e^{-\mu(\sigma_w/u_c)^2(\omega/\omega_w)^2} P_{33,\text{lf}}$$

$$P_{13}(\omega) = e^{-\mu[(\sigma_w\kappa_0)/\omega_w]^2[\omega/(u_c\kappa_0)]^2} P_{13,\text{lf}} = e^{-\mu(\sigma_w/u_c)^2\omega/\omega_w^2} P_{13,\text{lf}}, \quad (28)$$

where $P_{33,\text{lf}}$ and $P_{13,\text{lf}}$ are the spectral densities in the low-frequency flat parts of the autospectrum and cospectrum. Therefore, the low-frequency spectral shape

in the presence of waves can be represented by the constant spectral density at very low frequencies multiplied by a factor that decays exponentially with increasing frequency. The decay scale for the spectrum in dimensionless form is set by $\sigma_w \kappa_0 / \omega_w$. This exponential decay factor causes the shift of the apparent rolloff to lower frequency.

From Eq. (28), the apparent rolloff frequency in the dimensionless spectrum is

$$\frac{\omega_n}{u_c \kappa_0} = \left(\frac{\sigma_w \kappa_0}{\omega_w} \right)^{-1} \sqrt{-\frac{1}{\mu} \ln \left(\frac{n}{100} \right)}, \quad (29)$$

where $n = 100 P_{33}(\omega_n) / P_{33,lf}$ is the spectral density at the apparent rolloff frequency as a percentage of the spectral density for $\omega \rightarrow 0$ (e.g., $n = 90\%$ for ω_{90}). The values determined empirically from spectra agreed very well with Eq. (29) for $\sigma_w \kappa_0 / \omega_w > 1$ (Figs. 11b,d).

Equation (29) can be written in dimensional form as

$$\omega_n = \sqrt{-\frac{1}{\mu} \ln \left(\frac{n}{100} \right)} \left(\frac{\sigma_w}{u_c} \right)^{-1} \omega_w. \quad (30)$$

Therefore, the frequency at which the apparent low-frequency rolloff occurs in the presence of waves is proportional to the peak wave frequency and inversely proportional to σ_w / u_c . The apparent low-frequency rolloff is therefore independent of the true rolloff that occurs in the wavenumber spectrum at $\kappa \sim \kappa_0$.

4. Summary and conclusions

We have extended previous work that investigated the kinematic effects of wave advection on fixed-location observations of inertial subrange turbulence (Lumley and Terray 1983) by considering the complete range of turbulence length scales, from energy-containing scales to dissipative scales. Using model turbulence κ -spectrum shapes together with a general form of the frozen turbulence approximation, we investigated the effects of wave orbital motion on turbulence ω spectra across a wide parameter space that includes conditions typical in the coastal ocean, extending previous work (Gerbi et al. 2008) to situations where wave orbital velocities exceed the current. While we found that the high-wavenumber dissipation range has negligible effect on turbulence ω spectra across frequencies typically of interest, interaction between wave advection and the rolloff at energy-containing scales significantly affects the shapes of turbulence ω spectra.

We showed that the shapes of ω spectra can be expressed as a function of two key dimensionless parameters:

σ_w / u_c , the ratio of mean advection speed by waves to the current, and $u_c \kappa_0 / \omega_w$, the ratio of the time scale associated with waves to the time scale corresponding to advection of energy-containing turbulence by the current. The shape of the dimensionless spectrum at high frequencies is controlled primarily by the parameter σ_w / u_c , while the low-frequency spectral shape is controlled by $\sigma_w \kappa_0 / \omega_w$.

Our analyses illustrated the dependences of characteristic features of ω spectra on these dimensionless parameters (Table 2):

- 1) The offset due to waves of the $-5/3$ region of autospectra and the $-7/3$ region of cospectra is a function of σ_w / u_c only, illustrating that the rolloff and dissipation range have negligible effect on the inertial subrange in wave-affected ω spectra. Previously proposed methods for estimating dissipation rate (Trowbridge and Elgar 2001; Feddersen et al. 2007; Gerbi et al. 2009) are therefore expected to be robust across a wide range of conditions.
- 2) When $\sigma_w / u_c < 1$, the peak in the variance-preserving spectrum occurs at $\omega \sim u_c \kappa_0$ and is unaffected by wave advection. If $\sigma_w / u_c > 1$ and $\sigma_w \kappa_0 / \omega_w > 2$, the peak in the variance-preserving spectrum occurs at $\omega \sim \sigma_w \kappa_0$, corresponding to advection of energy-containing eddies at the rms wave orbital velocity. In these parameter ranges, turbulence length scales can be estimated from the frequency of the peak in the variance-preserving turbulence spectrum if the wave peak can first be adequately removed.
- 3) When the wave orbital excursion is smaller than energy-containing eddies ($\sigma_w \kappa_0 / \omega_w < 1$), the low-frequency rolloff in autospectra and cospectra is unaffected by wave advection and occurs at $\omega \sim u_c \kappa_0$. When $\sigma_w \kappa_0 / \omega_w > 1$, there is an apparent rolloff at $\omega \sim (\sigma_w / u_c)^{-1} \omega_w$. Previously proposed methods for estimating Reynolds stresses and turbulence length scales by fitting to model spectrum shapes to the low-frequency portion of ω spectra (Gerbi et al. 2008; Kirincich et al. 2010) should therefore only be used when $\sigma_w \kappa_0 / \omega_w < 1$ and $\sigma_w / u_c < 2$. For larger values of these parameters, the changes in the spectrum shape due to the wave advection derived in this study must be taken into account.

Our model results have revealed the characteristics of turbulence ω spectra that can be attributed to the purely kinematic process of advection by wave orbital motion. Because spectrum shapes collapse according to key dimensionless parameters, these parameters can be used to diagnose when wave advection needs to be taken into

account and its effects turbulence spectra. Although idealized, our model results provide insight into the interpretation fixed-location turbulence observations and a valuable point of comparison for the complex spectral shapes that are often computed from field measurements.

Acknowledgments. Funding for this work was provided by the National Science Foundation (1061108, 1435530). We are grateful to Falk Feddersen and an anonymous reviewer for their thoughtful comments that improved this manuscript.

APPENDIX

Expressions for the Shapes of Turbulence ω Spectra

a. Horizontal velocity autospectrum for isotropic turbulence

An expression for the spectral shape, in frequency space, can be derived by substituting the form of the wavenumber spectrum in Eqs. (12)–(13) into Eqs. (6), (8), and (10). The one-dimensional autospectrum for u_1 , along direction x_1 , in wavenumber space is

$$\begin{aligned} c_{11}(t) &= \int_0^\infty e^{i\omega t} \frac{S_{u_1 u_1}(\omega)}{\omega^2} d\omega \\ &= \left(\frac{\sigma_w}{\omega_w}\right)^2 \left(\frac{\omega_w}{u_c \kappa_0}\right)^2 \int_0^\infty e^{i[\omega/(u_c \kappa_0)] u_c \kappa_0 t} \frac{S_{u_1 u_1}^*[\omega/(u_c \kappa_0)]}{[\omega/(u_c \kappa_0)]^2} d[\omega/(u_c \kappa_0)] \\ &= \left(\frac{\sigma_w}{\omega_w}\right)^2 F_2(u_c \kappa_0 t). \end{aligned} \quad (\text{A3})$$

The term $S_{u_1 u_1}^*$ is the normalized, one-sided, wave orbital velocity spectrum formed by first nondimensionalizing frequency as $\omega/(u_c \kappa_0)$ and then dividing by the variance such that $\int_0^\infty S_{u_1 u_1}^*[\omega/(u_c \kappa_0)] d[\omega/(u_c \kappa_0)] = 1$. We define μ as

$$\begin{aligned} \mu &= \left(\frac{\sigma_w}{\omega_w}\right)^{-2} \int_0^\infty S_{x_1 x_1}(\omega) d\omega = \left(\frac{\sigma_w}{\omega_w}\right)^{-2} \int_0^\infty \frac{S_{u_1 u_1}(\omega)}{\omega^2} d\omega \\ &= \left(\frac{u_c \kappa_0}{\omega_w}\right)^{-2} \int_0^\infty \frac{S_{u_1 u_1}^*[\omega/(u_c \kappa_0)]}{[\omega/(u_c \kappa_0)]^2} d[\omega/(u_c \kappa_0)]. \end{aligned} \quad (\text{A4})$$

$$\begin{aligned} E_{11}(\kappa_1) &= \int_{\kappa_1}^\infty \frac{E(\kappa)}{\kappa} \left(1 - \frac{\kappa_1^2}{\kappa^2}\right) d\kappa \\ &= C \mathcal{E}^{2/3} \kappa_0^{-5/3} \int_{\kappa_1/\kappa_0}^\infty \frac{s'}{(s'^2 + 1)^{11/6}} \left[1 - \frac{(\kappa_1/\kappa_0)^2}{s'^2}\right] ds' \\ &= C \mathcal{E}^{2/3} \kappa_0^{-5/3} F_1(\kappa_1/\kappa_0). \end{aligned} \quad (\text{A1})$$

The integration variable is $s' = \kappa/\kappa_0$, and E_{11} is defined such that $\int_0^\infty E_{11}(\kappa_1) d\kappa_1 = \overline{u_1^2}$. Both E_{11} and F_1 are even functions, that is, $E_{11}(-\kappa_1) = E_{11}(\kappa_1)$.

Substituting Eq. (A1) into Eq. (10) yields the expression for the autocorrelation function for turbulent velocity fluctuations at a fixed location:

$$\begin{aligned} R_{11}(t) &= \frac{1}{2} \int_{-\infty}^\infty E_{11}(\kappa_1) e^{i\kappa_1 u_c t} e^{-\kappa_1 \kappa_1 [c_{11}(0) - c_{11}(t)]} d\kappa_1 \\ &= \frac{1}{2} C \mathcal{E}^{2/3} \kappa_0^{-2/3} \int_{-\infty}^\infty F_1(s) e^{i s u_c \kappa_0 t} e^{-\kappa_0^2 s^2 [c_{11}(0) - c_{11}(t)]} ds. \end{aligned} \quad (\text{A2})$$

Here, the integration variable is $s = \kappa_1/\kappa_0$.

From Eq. (6), the autocorrelation function for wave orbital excursions is

The term μ is a factor of order unity that depends on the shape of the wave orbital velocity spectrum. For narrowband waves, $\mu = 1$. From the above definitions, $F_2(0) = \mu$, and $\lim_{y \rightarrow \infty} F_2(y) = 0$. We also define $S_{x_1 x_1}^*[\omega/(u_c \kappa_0)] = S_{u_1 u_1}^*[\omega/(u_c \kappa_0)]/[\omega/(u_c \kappa_0)]^2$. Therefore, $\int_0^\infty S_{x_1 x_1}^*[\omega/(u_c \kappa_0)] d[\omega/(u_c \kappa_0)] = \mu [\omega_w/(u_c \kappa_0)]^{-2}$ and $c_{11}(0) = (\sigma_w/\omega_w)^2 [\omega_w/(u_c \kappa_0)]^2 \int_0^\infty S_{x_1 x_1}^*[\omega/(u_c \kappa_0)] d[\omega/(u_c \kappa_0)]$.

Substituting Eq. (A3) into Eq. (A2) gives

$$R_{11}(t) = \frac{1}{2} C \mathcal{E}^{2/3} \kappa_0^{-2/3} \int_{-\infty}^\infty F_1(s) e^{i s u_c \kappa_0 t} e^{-s^2 [(\sigma_w \kappa_0/\omega_w)]^2 [\mu - F_2(u_c \kappa_0 t)]} ds. \quad (\text{A5})$$

Now substituting Eq. (A5) into Eq. (8) gives

$$\begin{aligned}
 P_{11}(\omega) &= \frac{1}{2\pi} \int_{-\infty}^{\infty} e^{-i\omega t} R_{11}(t) dt \\
 &= \left(\frac{\varepsilon}{\kappa_0}\right)^{2/3} \frac{1}{u_c \kappa_0} \frac{C}{4\pi} \int_{-\infty}^{\infty} \int_{-\infty}^{\infty} F_1(s) e^{-i\{[\omega/(u_c \kappa_0)] - s\}y} e^{-[(u_c \kappa_0)/\omega_w]^2 (\sigma_w/u_c)^2 [\mu - F_2(y)]^2 s^2} ds dy \\
 &= \left(\frac{\varepsilon}{\kappa_0}\right)^{2/3} \frac{1}{u_c \kappa_0} F_3\left(\frac{\omega}{u_c \kappa_0}, \frac{u_c \kappa_0}{\omega_w}, \frac{\sigma_w}{u_c}, \mu\right),
 \end{aligned} \tag{A6}$$

where the integration variable $y = u_c \kappa_0 t$. The term P_{11} is defined such that $\int_{-\infty}^{\infty} P_{11}(\omega) d\omega = \overline{u_1^2}$. Equation (A6) gives the form of the dimensionless, two-sided spectrum in frequency space F_3 as a function of the two parameters $u_c \kappa_0/\omega_w$ and $\sigma_w \kappa_0/\omega_w$ and the wave spectrum shape factor μ .

1) HIGH-FREQUENCY LIMIT

For $\kappa/\kappa_0 \gg 1$ ($s' \gg 1$), for positive s , F_1 reduces to

$$F_1(s) = \int_s^{\infty} \text{sgn}(s') s'^{-8/3} \left(1 - \frac{s^2}{s'^2}\right) ds' = \frac{18}{55} s^{-5/3}. \tag{A7}$$

The term F_1 is even, so for negative s , $F_1(s) = 18/55 |s|^{-5/3}$. Following [Trowbridge and Elgar \(2001\)](#), in the limit of high frequencies (short times), the autocorrelation function can be expressed as

$$c_{11}(t) = \langle x_1(\tau) x_1(t + \tau) \rangle = \frac{\sigma_w^2}{\omega_w^2} \left[\mu - \frac{1}{2} \left(\frac{\omega_w}{u_c \kappa_0}\right)^2 (u_c \kappa_0 t)^2 \right]. \tag{A8}$$

This result is obtained by expanding x in a Taylor expansion around $x(\tau)$.

Substituting Eq. (A8) into Eq. (A6) and using the substitution $y = u_c \kappa_0 t$ yields

$$P_{11}(\omega) = \frac{1}{4\pi} \frac{18}{55} C \frac{1}{u_c \kappa_0} (\varepsilon/\kappa_0)^{2/3} \int_{-\infty}^{\infty} |s|^{-5/3} \int_{-\infty}^{\infty} e^{-i\{[\omega/(u_c \kappa_0)] - s\}y} e^{-(\sigma_w/u_c)^2 (1/2)y^2 s^2} ds dy. \tag{A9}$$

The integral with respect to y can be evaluated using standard integral tables, yielding

$$P_{11}(\omega) = \frac{\sqrt{2\pi}}{4\pi} \frac{18}{55} C \frac{1}{u_c \kappa_0} (\varepsilon/\kappa_0)^{2/3} (\sigma_w/u_c)^{-1} \int_{-\infty}^{\infty} |s|^{-8/3} \exp(-\{[\omega/(u_c \kappa_0)] - s\}^2/2 (\sigma_w/u_c)^2 s^2) ds.$$

Now using the variable substitution $\zeta = [\omega/(u_c \kappa_0)] s^{-1}$,

$$P_{11}(\omega) = \frac{1}{\sqrt{2\pi}} \frac{9}{55} C (\varepsilon u_c)^{2/3} |\omega|^{-5/3} (\sigma_w/u_c)^{-1} \int_{-\infty}^{\infty} |\zeta|^{2/3} e^{-(1/2)(\sigma_w/u_c)^{-2} (1-\zeta)^2} d\zeta,$$

and substituting $\chi = (u_c/\sigma_w)(1 - \zeta)$ gives

$$P_{11}(\omega) = \frac{9}{55} C (\varepsilon u_c)^{2/3} |\omega|^{-5/3} \frac{1}{\sqrt{2\pi}} \int_{-\infty}^{\infty} \left|1 - \frac{\sigma_w}{u_c} \chi\right|^{2/3} e^{-(1/2)\chi^2} d\chi = \frac{9}{55} C (\varepsilon u_c)^{2/3} |\omega|^{-5/3} I, \tag{A10}$$

where $I = (1/\sqrt{2\pi}) \int_{-\infty}^{\infty} |1 - (\sigma_w/u_c)\chi|^{2/3} e^{-(1/2)\chi^2} d\chi$. The expression for the $-5/3$ region in the absence of waves is

$$P_{11}(\omega) = \frac{1}{2} E_{11}[\kappa_1(\omega)] \frac{d\kappa_1}{d\omega} = \frac{9}{55} C (\varepsilon u_c)^{2/3} |\omega|^{-5/3}. \tag{A11}$$

Therefore, the spectral density is increased by a factor I by wave advection. This and similar expressions have been used previously to calculate dissipation rates from $-5/3$ fits to spectra in the presence of waves (e.g., [Trowbridge and Elgar 2001](#)).

2) LOW-FREQUENCY LIMIT

We now consider the apparent rolloff at frequencies $\omega < \omega_w$. Assuming $S_{x_1x_1}^*$ is Gaussian [Eq. (17)],

$$S_{x_1x_1}^*[\omega/(u_c\kappa_0)] = \mu[\omega_w/(u_c\kappa_0)]^{-2} \frac{1}{\sqrt{2\pi}(\Delta\omega_w/\omega_w)[\omega_w/(u_c\kappa_0)]} \exp\left\{-\frac{[\omega/(u_c\kappa_0) - \omega_w/(u_c\kappa_0)]^2}{2(\Delta\omega_w/\omega_w)^2[\omega_w/(u_c\kappa_0)]^2}\right\}.$$

From Eq. (A3), using standard integral tables,

$$\begin{aligned} F_2(y) &= [\omega_w/(u_c\kappa_0)]^2 \int_0^\infty e^{i[\omega/(u_c\kappa_0)]y} S_{x_1x_1}^*[\omega/(u_c\kappa_0)] d[\omega/(u_c\kappa_0)] \\ &= \frac{\mu}{\sqrt{2\pi}(\Delta\omega_w/\omega_w)[\omega_w/(u_c\kappa_0)]} \int_0^\infty e^{i[\omega/(u_c\kappa_0)]y} \exp\left\{-\frac{[\omega/(u_c\kappa_0) - \omega_w/(u_c\kappa_0)]^2}{2(\Delta\omega_w/\omega_w)^2[\omega_w/(u_c\kappa_0)]^2}\right\} d[\omega/(u_c\kappa_0)] \\ &= \mu e^{i[\omega_w/(u_c\kappa_0)]y} e^{-(1/2)(\Delta\omega_w/\omega_w)^2[\omega_w/(u_c\kappa_0)]^2 y^2}. \end{aligned} \quad (\text{A12})$$

For $(\Delta\omega_w/\omega_w)[\omega_w/(u_c\kappa_0)] > 1$, F_2 decays to zero quickly with increasing y . The term F_2 decays to zero more quickly and with fewer oscillations for broadband than narrowband waves.

The ratio of the spectral density at frequency ω relative to its constant value at small ω is

$$\begin{aligned} \frac{P_{11}(\omega)}{P_{11,\text{lf}}} &= \frac{\int_{-\infty}^\infty \int_{-\infty}^\infty F_1(s) e^{-i\{[\omega/(u_c\kappa_0)]-s\}y} e^{-s^2[(\sigma_w\kappa_0)/\omega_w]^2[\mu-F_2(y)]} ds dy}{\int_{-\infty}^\infty \int_{-\infty}^\infty F_1(s) e^{isy} e^{-s^2[(\sigma_w\kappa_0)/\omega_w]^2[\mu-F_2(y)]} ds dy} \\ &= \frac{\int_{-\infty}^\infty \int_{-\infty}^\infty F_1(s) e^{-i\{[\omega/(u_c\kappa_0)]-s\}y} e^{-s^2[(\sigma_w\kappa_0)/\omega_w]^2\mu(1-\exp\{i[\omega_w/(u_c\kappa_0)]y\})} \exp\{-(1/2)(\Delta\omega_w/\omega_w)^2[\omega_w/(u_c\kappa_0)]^2 y^2\}} ds dy}{\int_{-\infty}^\infty \int_{-\infty}^\infty F_1(s) e^{isy} e^{-s^2[(\sigma_w\kappa_0)/\omega_w]^2\mu(1-\exp\{i[\omega_w/(u_c\kappa_0)]y\})} \exp\{-(1/2)(\Delta\omega_w/\omega_w)^2[\omega_w/(u_c\kappa_0)]^2 y^2\}} ds dy}. \end{aligned}$$

Using the variable substitutions $\zeta = [\omega_w/(u_c\kappa_0)]y$ and $\chi = [\omega_w/(u_c\kappa_0)]^{-1}\{s - [\omega/(u_c\kappa_0)]\}$,

$$\begin{aligned} \frac{P_{11}(\omega)}{P_{11,\text{lf}}} &= \frac{\int_{-\infty}^\infty F_1\{[\omega_w/(u_c\kappa_0)]\chi + [\omega/(u_c\kappa_0)]\} \int_{-\infty}^\infty e^{i\chi\zeta} e^{-\{[\omega_w/(u_c\kappa_0)]\chi + [\omega/(u_c\kappa_0)]\}^2[(\sigma_w\kappa_0)/\omega_w]^2\mu\{1-\exp(i\zeta)\exp[-(1/2)(\Delta\omega_w/\omega_w)^2\zeta^2]\}} d\zeta d\chi}{\int_{-\infty}^\infty F_1\{[\omega_w/(u_c\kappa_0)]\chi\} \int_{-\infty}^\infty e^{i\chi\zeta} e^{-\chi^2[\omega_w/(u_c\kappa_0)]^2[(\sigma_w\kappa_0)/\omega_w]^2\mu\{1-\exp(i\zeta)\exp[-(1/2)(\Delta\omega_w/\omega_w)^2\zeta^2]\}} d\zeta d\chi} \\ &= e^{-\mu[(\sigma_w\kappa_0)/\omega_w]^2[\omega/(u_c\kappa_0)]^2} \left(\frac{\int_{-\infty}^\infty F_1\{[\omega_w/(u_c\kappa_0)]\chi + (\omega/\omega_w)\} e^{-\mu(\sigma_w/u_c)^2[\chi + (\omega/\omega_w)]^2} \exp(i\zeta)\exp[-(1/2)(\Delta\omega_w/\omega_w)^2\zeta^2] d\zeta d\chi}{\int_{-\infty}^\infty F_1\{[\omega_w/(u_c\kappa_0)]\chi\} e^{-\mu(\sigma_w/u_c)^2\chi^2} \int_{-\infty}^\infty e^{i\chi\zeta} e^{\mu(\sigma_w/u_c)^2\chi^2} \exp(i\zeta)\exp[-(1/2)(\Delta\omega_w/\omega_w)^2\zeta^2] d\zeta d\chi} \right) \\ &\approx e^{-\mu[(\sigma_w\kappa_0)/\omega_w]^2[\omega/(u_c\kappa_0)]^2}. \end{aligned} \quad (\text{A13})$$

In the last step, we assumed $F_1\{[\omega_w/(u_c\kappa_0)]\chi + [\omega/(u_c\kappa_0)]\} \approx F_1\{[\omega_w/(u_c\kappa_0)]\chi\}$. The rolloff in $F_1(s)$ occurs at $s = 1$. Since the exponential in the outside integral has decay scale $[\mu^{1/2}(\sigma_w/u_c)]^{-1} \approx (\sigma_w/u_c)^{-1}$, the integrand is dominated by $\chi < (\sigma_w/u_c)^{-1}$ or equivalently $[\omega_w/(u_c\kappa_0)]\chi < [\omega_w/(\sigma_w\kappa_0)]$. The assumption $F_1\{[\omega_w/(u_c\kappa_0)]\chi + [\omega/(u_c\kappa_0)]\} \approx F_1\{[\omega_w/(u_c\kappa_0)]\chi\}$ is therefore reasonable if both $\omega/(u_c\kappa_0) \ll 1$ and $\omega_w/(\sigma_w\kappa_0) < 1$.

From Eq. (A13), $\omega/(u_c\kappa_0) \ll 1$ is guaranteed if

$$\begin{aligned} \frac{P_{11}(\omega_n)}{P_{11,\text{lf}}} &= \frac{n}{100} = e^{-\mu[(\sigma_w\kappa_0)/\omega_w]^2[\omega_n/(u_c\kappa_0)]^2} \\ &\gg e^{-\mu[(\sigma_w\kappa_0)/\omega_w]^2} \\ \frac{\sigma_w\kappa_0}{\omega_w} &\gg \left[-\frac{1}{\mu} \ln\left(\frac{n}{100}\right) \right]^{1/2}, \end{aligned} \quad (\text{A14})$$

where n is the spectral density at frequency ω_n as a percentage of the spectral density for $\omega \rightarrow 0$. For $n = 90$,

Eq. (A14) yields $(\sigma_w \kappa_0)/\omega_w \gg 0.3$. Therefore, for $n = 90$, all these criteria are satisfied if $(\sigma_w \kappa_0)/\omega_w > 1$, that is, if the wave orbital excursion is larger than the energy-containing turbulent eddies.

b. Vertical velocity autospectrum for isotropic turbulence

The 1D autospectrum for u_3 along direction x_1 in wavenumber space is

$$\begin{aligned}
 E_{33}(\kappa_1) &= \frac{1}{2} \left[E_{11}(\kappa_1) - \kappa_1 \frac{dE_{11}}{d\kappa_1} \right] \\
 &= \frac{1}{2} C \varepsilon^{2/3} \kappa_0^{-5/3} \left\{ \int_{\kappa_1/\kappa_0}^{\infty} \frac{s'}{(s'^2 + 1)^{11/6}} \left[1 - \frac{(\kappa_1/\kappa_0)^2}{s'^2} \right] ds' - \frac{\kappa_1}{\kappa_0} \frac{d}{d(\kappa_1/\kappa_0)} \int_{\kappa_1/\kappa_0}^{\infty} \frac{s'}{(s'^2 + 1)^{11/6}} \left[1 - \frac{(\kappa_1/\kappa_0)^2}{s'^2} \right] ds' \right\} \\
 &= \frac{1}{2} C \varepsilon^{2/3} \kappa_0^{-5/3} \int_{\kappa_1/\kappa_0}^{\infty} \frac{s'}{(s'^2 + 1)^{11/6}} \left[1 + \frac{(\kappa_1/\kappa_0)^2}{s'^2} \right] ds' \\
 &= C \varepsilon^{2/3} \kappa_0^{-5/3} G_1(\kappa_1/\kappa_0).
 \end{aligned} \tag{A15}$$

The remainder of the analysis follows that for the u_1 autospectrum. The final result is given in Eqs. (21) and (22).

1) HIGH-FREQUENCY LIMIT

The only difference between the high-frequency limit for vertical and horizontal velocity components is the difference between F_1 and G_1 . In the high-frequency limit,

$$G_1(s) = \frac{1}{2} \int_s^{\infty} |s'|^{-8/3} \left(1 + \frac{s'^2}{s^2} \right) ds' = \frac{24}{55} |s|^{-5/3}. \tag{A16}$$

Therefore, in the high-frequency limit,

$$P_{33}(\omega) = \frac{12}{55} C (\varepsilon u_c)^{2/3} \omega^{-5/3} I, \tag{A17}$$

where I is the same as for the horizontal velocity autospectrum [Eq. (A10)].

2) LOW-FREQUENCY LIMIT

The derivation for the low-frequency apparent rolloff in the vertical velocity autospectrum follows that for the horizontal spectrum exactly. For low frequencies, the spectral density at frequency ω relative to its constant value for very low frequencies is

$$\frac{P_{33}(\omega)}{P_{33,lf}} \approx e^{-\mu [(\sigma_w \kappa_0)/\omega_w]^2 [\omega/(u_c \kappa_0)]^2}. \tag{A18}$$

c. Cospectrum for anisotropic turbulence

The equation for the one-sided cospectrum in wave-number space is

$$E_{13}(\kappa_1) = \frac{\overline{u'_1 u'_3}}{\kappa_0} \frac{7}{3\pi} \sin\left(\frac{3\pi}{7}\right) \frac{1}{1 + |\kappa_1/\kappa_0|^{7/3}}. \tag{A19}$$

Substituting this into Eq. (10) yields

$$\begin{aligned}
 R_{13}(t) &= \frac{1}{2} \int_{-\infty}^{\infty} E_{13}(\kappa_1) e^{-i\kappa_1 u_c t} e^{-\kappa_1 \kappa_1 [c_{11}(0) - c_{11}(t)]} d\kappa_1 \\
 &= \overline{u'_1 u'_3} \frac{7}{6\pi} \sin\left(\frac{3\pi}{7}\right) \int_{-\infty}^{\infty} \frac{1}{1 + |s|^{7/3}} e^{-i\kappa_0 u_c t s} e^{-s^2 \kappa_0^2 [c_{11}(0) - c_{11}(t)]} ds,
 \end{aligned} \tag{A20}$$

where $s = \kappa_1/\kappa_0$. Substituting Eq. (A3) into Eq. (A20) gives

$$R_{13}(t) = \overline{u'_1 u'_3} \frac{7}{6\pi} \sin\left(\frac{3\pi}{7}\right) \int_{-\infty}^{\infty} \frac{1}{1 + |s|^{7/3}} e^{-i\kappa_0 u_c t s} e^{-s^2 [(\sigma_w \kappa_0)/\omega_w]^2 [\mu - F_2(u_c \kappa_0 t)]} ds. \tag{A21}$$

Now, substituting this into Eq. (8) with the variable substitution $y = u_c \kappa_0 t$ yields

$$\begin{aligned}
P_{13}(\omega) &= \frac{1}{2\pi} \int_{-\infty}^{\infty} e^{-i\omega t} R_{13}(t) dt \\
&= \frac{\overline{u'_1 u'_3}}{u_c \kappa_0} \frac{7}{12\pi^2} \sin\left(\frac{3\pi}{7}\right) \int_{-\infty}^{\infty} \int_{-\infty}^{\infty} \frac{1}{1 + |s|^{7/3}} e^{-i\{[\omega/(u_c \kappa_0)] - s\}y} e^{-[(u_c \kappa_0)/\omega_w]^2 (\sigma_w/u_c)^2 [\mu - F_2(y)]^2 s^2} ds dy \\
&= \frac{\overline{u'_1 u'_3}}{u_c \kappa_0} H_3\left(\frac{\omega}{u_c \kappa_0}, \frac{u_c \kappa_0}{\omega_w}, \frac{\sigma_w}{u_c}, \mu\right). \tag{A22}
\end{aligned}$$

1) HIGH-FREQUENCY LIMIT

The offset of the $-7/3$ region of cospectra can be derived in a similar way to the offset of the $-5/3$ region of autospectra. Substituting Eq. (A9) into Eq. (A22) yields

$$P_{13}(\omega) = \frac{\overline{u'_1 u'_3}}{u_c \kappa_0} \frac{7}{12\pi^2} \sin\left(\frac{3\pi}{7}\right) \int_{-\infty}^{\infty} \int_{-\infty}^{\infty} \frac{1}{1 + |s|^{7/3}} e^{-i\{[\omega/(u_c \kappa_0)] - s\}y} e^{-(1/2)(\sigma_w/u_c)^2 s^2 y^2} ds dy.$$

In the limit of high wavenumbers ($s \gg 1$), this expression reduces to

$$P_{13}(\omega) = \frac{\overline{u'_1 u'_3}}{u_c \kappa_0} \frac{7}{12\pi^2} \sin\left(\frac{3\pi}{7}\right) \int_{-\infty}^{\infty} |s|^{-7/3} \int_{-\infty}^{\infty} e^{-i\{[\omega/(u_c \kappa_0)] - s\}y} e^{-(1/2)(\sigma_w/u_c)^2 s^2 y^2} dy ds.$$

The integral with respect to y can be evaluated using standard integral tables, yielding

$$P_{13}(\omega) = \frac{\overline{u'_1 u'_3}}{u_c \kappa_0} \frac{7}{6\pi\sqrt{2\pi}} \sin\left(\frac{3\pi}{7}\right) \left(\frac{\sigma_w}{u_c}\right)^{-1} \int_{-\infty}^{\infty} |s|^{-10/3} e^{-(1/2)(\sigma_w/u_c)^{-2} \{[\omega/(u_c \kappa_0)](1/s) - 1\}^2} ds.$$

Now using the variable substitution $\zeta = [\omega/(u_c \kappa_0)](1/s)$,

$$P_{13}(\omega) = -\frac{\overline{u'_1 u'_3}}{u_c \kappa_0} \frac{7}{6\pi\sqrt{2\pi}} \sin\left(\frac{3\pi}{7}\right) \left(\frac{\sigma_w}{u_c}\right)^{-1} \left|\frac{\omega}{\kappa_0 u_c}\right|^{-7/3} \int_{-\infty}^{\infty} |\zeta|^{4/3} \exp[-(1/2)(\sigma_w/u_c)^{-2}(\zeta - 1)^2] d\zeta,$$

and substituting $\chi = (u_c/\sigma_w)(1 - \zeta)$ gives

$$\begin{aligned}
P_{13}(\omega) &= \frac{\overline{u'_1 u'_3}}{u_c \kappa_0} \frac{7}{6\pi} \sin\left(\frac{3\pi}{7}\right) \left|\frac{\omega}{\kappa_0 u_c}\right|^{-7/3} \frac{1}{\sqrt{2\pi}} \int_{-\infty}^{\infty} \left|1 - \frac{\sigma_w}{u_c} \chi\right|^{4/3} e^{-(1/2)\chi^2} d\chi \\
&= \frac{\overline{u'_1 u'_3}}{u_c \kappa_0} \frac{7}{6\pi} \sin\left(\frac{3\pi}{7}\right) \left|\frac{\omega}{\kappa_0 u_c}\right|^{-7/3} J\left(\frac{\sigma_w}{u_c}\right), \tag{A23}
\end{aligned}$$

where

$$J(\sigma_w/u_c) = (1/\sqrt{2\pi}) \int_{-\infty}^{\infty} |1 - (\sigma_w/u_c)\chi|^{4/3} \exp[-(1/2)\chi^2] d\chi.$$

Comparing with the expression for no waves,

$$P_{13}(\omega) = \frac{\overline{u'_1 u'_3}}{u_c \kappa_0} \frac{7}{6\pi} \sin\left(\frac{3\pi}{7}\right) \left|\frac{\omega}{u_c \kappa_0}\right|^{-7/3}. \tag{A24}$$

Therefore, J is the ratio of the spectral density in the $-7/3$ region in the presence of waves to that in the absence of waves and is analogous to I for isotropic turbulence autospectra.

2) LOW-FREQUENCY LIMIT

The derivation for the apparent rolloff in P_{13} at frequencies $\omega < \omega_w$ follows the corresponding derivation for P_{11} exactly. In the low-frequency limit,

$$\frac{P_{13}(\omega)}{P_{13,lf}} \approx e^{-\mu[(\sigma_w \kappa_0)/\omega_w]^2 [\omega/(u_c \kappa_0)]^2}. \quad (\text{A25})$$

REFERENCES

- Benilov, A. Y., and B. N. Filyushkin, 1970: Application of methods of linear filtration to an analysis of fluctuations in the surface layer of the sea. *Izv., Atmos. Ocean. Phys.*, **6**, 810–819.
- Feddersen, F., 2010: Quality controlling surf zone acoustic Doppler velocimeter observations to estimate the turbulent dissipation rate. *J. Atmos. Oceanic Technol.*, **27**, 2039–2055, doi:10.1175/2010JTECHO783.1.
- , 2012: Observations of the surf-zone turbulent dissipation rate. *J. Phys. Oceanogr.*, **42**, 386–399, doi:10.1175/JPO-D-11-082.1.
- , and A. J. Williams III, 2007: Direct estimation of the Reynolds stress vertical structure in the nearshore. *J. Atmos. Oceanic Technol.*, **24**, 102–116, doi:10.1175/JTECH1953.1.
- , J. H. Trowbridge, and A. J. Williams III, 2007: Vertical structure of dissipation in the nearshore. *J. Phys. Oceanogr.*, **37**, 1764–1777, doi:10.1175/JPO3098.1.
- Gerbi, G. P., J. H. Trowbridge, J. B. Edson, A. J. Plueddemann, E. A. Terray, and J. J. Fredericks, 2008: Measurements of momentum and heat transfer across the air–sea interface. *J. Phys. Oceanogr.*, **38**, 1054–1072, doi:10.1175/2007JPO3739.1.
- , —, E. A. Terray, A. J. Plueddemann, and T. Kukulka, 2009: Observations of turbulence in the ocean surface boundary layer: Energetics and transport. *J. Phys. Oceanogr.*, **39**, 1077–1096, doi:10.1175/2008JPO4044.1.
- Geyer, W. R., J. H. Trowbridge, and M. M. Bowen, 2000: The dynamics of a partially mixed estuary. *J. Phys. Oceanogr.*, **30**, 2035–2048, doi:10.1175/1520-0485(2000)030<2035:TDOAPM>2.0.CO;2.
- Jones, N. L., and S. G. Monismith, 2008: The influence of white-capping waves on the vertical structure of turbulence in a shallow estuarine embayment. *J. Phys. Oceanogr.*, **38**, 1563–1580, doi:10.1175/2007JPO3766.1.
- Kaimal, J. C., J. C. Wyngaard, Y. Izumi, and O. R. Cote, 1972: Spectral characteristics of surface layer turbulence. *Quart. J. Roy. Meteor. Soc.*, **98**, 563–589, doi:10.1002/qj.49709841707.
- Kirincich, A. R., S. J. Lentz, and G. P. Gerbi, 2010: Calculating Reynolds stresses from ADCP measurements in the presence of surface waves using the cospectra-fit method. *J. Atmos. Oceanic Technol.*, **27**, 889–907, doi:10.1175/2009JTECHO682.1.
- Lentz, S. J., R. T. Guza, S. Elgar, F. Feddersen, and T. H. C. Herbers, 1999: Momentum balances on the North Carolina inner shelf. *J. Geophys. Res.*, **104**, 18 205–18 226, doi:10.1029/1999JC900101.
- Lumley, J. L., and E. A. Terray, 1983: Kinematics of turbulence connected by a random wave field. *J. Phys. Oceanogr.*, **13**, 2000–2007, doi:10.1175/1520-0485(1983)013<2000:KOTCBA>2.0.CO;2.
- Pope, S. B., 2000: *Turbulent Flows*. Cambridge University Press, 771 pp.
- Rosman, J. H., J. L. Hench, J. R. Koseff, and S. G. Monismith, 2008: Extracting Reynolds stresses from acoustic Doppler current profiler measurements in wave-dominated environments. *J. Atmos. Oceanic Technol.*, **25**, 286–306, doi:10.1175/2007JTECHO525.1.
- Shaw, W. J., and J. H. Trowbridge, 2001: The direct estimation of near-bottom turbulent fluxes in the presence of energetic wave motions. *J. Atmos. Oceanic Technol.*, **18**, 1540–1557, doi:10.1175/1520-0426(2001)018<1540:TDEONB>2.0.CO;2.
- Taylor, G. I., 1938: The spectrum of turbulence. *Proc. Roy. Soc. London*, **A164**, 476–490, doi:10.1098/rspa.1938.0032.
- Trowbridge, J. H., and S. Elgar, 2001: Turbulence measurements in the surf zone. *J. Phys. Oceanogr.*, **31**, 2403–2417, doi:10.1175/1520-0485(2001)031<2403:TMITSZ>2.0.CO;2.
- , and —, 2003: Spatial scales of stress-carrying nearshore turbulence. *J. Phys. Oceanogr.*, **33**, 1122–1128, doi:10.1175/1520-0485(2003)033<1122:SSOSNT>2.0.CO;2.
- Wyngaard, J. C., and S. F. Clifford, 1977: Taylor’s hypothesis and high-frequency turbulence spectra. *J. Atmos. Sci.*, **34**, 922–929, doi:10.1175/1520-0469(1977)034<0922:THAHTS>2.0.CO;2.